Acta Oceanol. Sin., 2022, Vol. 41, No. 9, P. 86–106
https://doi.org/10.1007/s13131-022-1992-6
http://www.aosocean.com
E-mail: ocean2@hyxb.org.cn

Distribution characteristics of delta reservoirs reshaped by bottom currents: A case study from the second member of the Yinggehai Formation in the DF1-1 gas field, Yinggehai Basin, South China Sea

Shuo Chen[1], Renhai Pu[1]*, Huiqiong Li[2], Hongjun Qu[1], Tianyu Ji[3], Siyu Su[1], Yunwen Guan[1], Hui Zhang[4]

[1] State Key Laboratory of Continental Dynamics (Northwest University), Xi'an 710069, China

[2] Research Institute of Yanchang Petroleum Group Co. Ltd., Xi'an 710065, China

[3] Research Institute of Petroleum Exploration and Development, Beijing 100083, China

[4] Research Institute of Zhanjiang Branch of China National Offshore Oil Corporation, Zhanjiang 524057, China

Received 6 May 2021; accepted 10 November 2021

Abstract

The Dongfang1-1 gas field (DF1-1) in the Yinggehai Basin is currently the largest offshore self-developed gas field in China and is rich in oil and gas resources. The second member of the Pliocene Yinggehai Formation (YGHF) is the main gas-producing formation and is composed of various sedimentary types; however, a clear understanding of the sedimentary types and development patterns is lacking. Here, typical lithofacies, logging facies and seismic facies types and characteristics of the YGHF are identified based on high-precision 3D seismic data combined with drilling, logging, analysis and testing data. Based on 3D seismic interpretation and attribute analysis, the origin of high-amplitude reflections is clarified, and the main types and evolution characteristics of sedimentary facies are identified. Taking gas formation upper II (IIU) as an example, the plane distribution of the delta front and bottom current channel is determined; finally, a comprehensive sedimentary model of the YGHF second member is established. This second member is a shallowly buried "bright spot" gas reservoir with weak compaction. The velocity of sandstone is slightly lower than that of mudstone, and the reflection has medium amplitude when there is no gas. The velocity of sandstone decreases considerably after gas accumulation, resulting in an increase in the wave impedance difference and high-amplitude (bright spot) reflection between sandstone and mudstone; the range of high amplitudes is consistent with that of gas-bearing traps. The distribution of gas reservoirs is obviously controlled by dome-shaped diapir structural traps, and diapir faults are channels through which natural gas from underlying Miocene source rocks can enter traps. The study area is a delta front deposit developed on a shallow sea shelf. The lithologies of the reservoir are mainly composed of very fine sand and coarse silt, and a variety of sedimentary structural types reflect a shallow sea delta environment; upward thickening funnel type, strong toothed bell type and toothed funnel type logging facies are developed. In total, 4 stages of delta front sand bodies (corresponding to progradational reflection seismic facies) derived from the Red River and Blue River in Vietnam have developed in the second member of the YGHF; these sand bodies are dated to 1.5 Ma and correspond to four gas formations. During sedimentation, many bottom current channels (corresponding to channel fill seismic facies) formed, which interacted with the superposed progradational reflections. When the provenance supply was strong in the northwest, the area was dominated by a large set of delta front deposits. In the period of relative sea level rise, surface bottom currents parallel to the coastline were dominant, and undercutting erosion was obvious, forming multistage superimposed erosion troughs. Three large bottom current channels that developed in the late sedimentary period of gas formation IIU are the most typical.

Key words: South China Sea, Yinggehai Basin, second member of the Yinggehai Formation, bottom current transformation, sedimentary model

Citation: Chen Shuo, Pu Renhai, Li Huiqiong, Qu Hongjun, Ji Tianyu, Su Siyu, Guan Yunwen, Zhang Hui. 2022. Distribution characteristics of delta reservoirs reshaped by bottom currents: A case study from the second member of the Yinggehai Formation in the DF1-1 gas field, Yinggehai Basin, South China Sea. Acta Oceanologica Sinica, 41(9): 86–106, doi: 10.1007/s13131-022-1992-6

1 Introduction

The Yinggehai Basin (YGHB), located in the South China Sea (SCS), is one of the world's eight offshore overpressurized basins and contains abundant natural gas resources. After more than 30 years of exploration, several commercial natural gas reservoirs and petroliferous structures have been found in the basin, including Dongfang (DF)1-1, DF29-1, DF1-13-1, and DF1-13-2 in the DF area and Ledong (LD)15-1 and LD22-1 in the Ledong area. The main gas reservoirs discovered to date are the shallow Yinggehai and Ledong formations at normal temperatures and

Foundation item: The National Natural Science Foundation of China's Major Project "Research on Geophysical Theories and Methods of Unconventional Oil and Gas Exploration and Development", Task I: "China's Tight Oil and Gas Reservoir Geological Characteristics, Classification and Typical Geological Model Establishment" under contract No. 41390451.
*Corresponding author, E-mail: purenhai@126.com

pressures and the Meishan Formation at high temperatures and pressures. In recent years, during the exploration of deep high-temperature and overpressurized strata, a large lithologic-tectonic composite gas field was discovered in the first member of the upper Miocene Huangliu Formation (Xie and Huang, 2014; Yang et al., 2013). The second member of the Yinggehai Formation (YGHF), as the main gas-producing formation in the shallow strata of the basin, is currently divided into four gas formations (submembers): I, upper II (IIU), lower II (IIL) and upper III (IIIU).

Different scholars have studied the sedimentary system of the second member of the YGHF in the DF gas field from various perspectives. Lü (2002) compared international examples with similar backgrounds and concluded that the DF1-1-1 gas field features many types of lowstand sedimentary systems, such as divergent and convergent types, under the influence of eastern and western provenances in addition to the long-axis transport of sediments of Red River provenance. Wang et al. (2008) divided the second member of the YGHF into six gas formations, namely, IV, III_L, III_U, II_L, II_U, and I, during the fine-scale reservoir description of the DF1-1-1 gas field. The gas-producing sections are gas formations I–IIIU. Jiang et al. (2012) reported that the second member of the YGHF mainly features the lower nearshore microfacies and offshore subfacies from bottom to top. Li et al. (2010) considered that the gas field as a whole was in the nearshore-offshore transition zone, mainly developing sand bars and beach sand bodies. Yue et al. (2017, 2018) studied the factors that controlled the formation of sedimentary facies in the DF1-1-1 gas field and pointed out that gas formations III and II mainly feature submarine fan turbidite sheet sands from the western provenance, gas formation I features offshore beach bar deposits, and offshore mud was deposited in each period.

Multistage erosion channels are found in the sedimentary system of the second member of the YGHF that developed alternately with underlying sand bodies in the study area. These channels spread along the coastline and cut the connected sand bodies into isolated mound sand bodies, increasing the heterogeneity of sandstone reservoirs. There are several interpretations of the genesis of erosion channels in marine sediments, such as mud flow gullies, lateral accretion complexes, bottom current channels, internal waves and internal tides. Zhuo et al. (2013) considered that this kind of channel is a large gravity flow channel developed on the western edge of the central diapir in the middle and later periods of the YGHF. Its high curvature is very similar to that of the lateral accretion complex proposed by Abreu et al. (2003) in a study of the evolution of the lower Miocene deep-water channel in the Angela Basin, West Africa, and this channel can be treated as a new oil and gas reservoir unit. Li et al. (2010) named this kind of erosion channel a “mud flow gully”, which is similar to an undercut channel caused by the slippage of sediments with loose grains and high argillaceous contents induced by a certain mechanism; such gullies are formed at the turning point of coastal and shallow sea topography and dominated by mudstone fills. Internal waves and internal tides usually occur during sea level rise and are very common in deep-water marine environments. These currents can cause a certain scale of bidirectional flow in the valleys and canyon channels formed by early gravity flows (Gao et al., 2000) and transport muddy, silty, and even fine sand-sized sediments with a velocity of 0.2–0.5 m/s (Mullins et al., 1982), mainly developing bidirectional cross-bedding (He et al., 2007). In addition, multistage bottom current sediments have been confirmed to have developed in the Zhujiang River Mouth Basin (ZRMB) and Qiongdongnan Basin (QDNB) since the late early Miocene to middle Miocene Meishan Formation sedimentary period in the northern SCS (Zheng and Yan, 2012; Li et al., 2013; Tian et al., 2015; Zheng et al., 2016; Sun et al., 2017), but there have been no reports on bottom currents in the YGHB.

At present, many controversies remain regarding the sedimentary facies of the second member of the YGHF, and there are few relevant reports in the international literature. The sedimentary model established based on previous research does not meet the needs of fine tapping potential in the later stage of development; the distribution of dominant facies zones in the unused area is not clear, and the research accuracy urgently needs to be improved. Therefore, determining the sedimentary facies types of each gas formation and the distribution of sandstone reservoirs is very important. The high-precision 3D seismic data and valuable marine drilling coring data in the YGHB provide an excellent opportunity for the study of these problems, including (1) clarifying the genesis and geological meaning of special seismic reflections in target strata; (2) analyzing the sedimentary types, evolution and distribution characteristics of each gas formation; and (3) establishing an integrated sedimentary model. The current research results help to better understand the sedimentary system of the second member of the YGHF in the DF gas field and provide a reference for the global exploration and development of oil and gas resources in shallow sea confined basins influenced by diverse sedimentary processes.

2 Geological setting

The YGHB is located on the northern continental margin of the SCS and lies in the Yinggehai Sea area between Hainan Island and the Indo-China Peninsula. The basin is a rhombus with a long axis extending NNW–SSE (Fig. 1a), and it is approximately 750 km long and 200 km wide, with an area of approximately 12.7×10^4 km^2 (Wang et al., 2013). The YGHB is connected with the Beibuwan Basin in the north, the Kunsong Uplift in the northwest, and the QDNB in the southeast by nearly vertical fault No. 1 (Sun et al., 2015). The basin can be divided into three first-order tectonic units: the central depression belt, the eastern Yinggehai slope belt and the western Yinggehai slope belt (Hao et al., 1996; Li et al., 1999; Huang et al., 2005; Xie et al., 2006) (Fig. 1a). The tectonic evolution of the basin can be divided into two main stages: the synrift stage and the postrift depression stage, with four substages corresponding to rift depression, fault depression, postrift thermal subsidence and postrift accelerated subsidence from bottom to top (Lei et al., 2015; Huang et al., 2018) (Fig. 1c).

The DF1-1 gas field (DF1-1) is located in the northwestern YGHB and north of the mud diapir structure belt in the central depression (Figs 1a, b). The gas field is a large simple short-axis anticline structure associated with a mud diapir and was discovered in 1992. The average water depth of DF1-1-1 is approximately 67 m, the superimposed gas-bearing area is over 309.27 km^2, and the geological reserves are greater than 100×10^8 m^3. It is currently the largest offshore independently developed gas field in China (Wang and Huang, 2008). At present, the second member of the YGHF is divided into four gas formations, namely, I, IIU, IIL and IIIU, which are also the target strata of this paper.

Previous studies have mainly focused on the provenance (Wang et al., 2014, 2015, 2019; Cao et al., 2015; Jiang et al., 2015), source rocks, reservoirs, cap rocks, migration and accumulation mechanisms and other factors related to the YGHB since the Cenozoic (Hao et al., 1995, 1996, 1998, 2000, 2002, 2004; Zhang and Hao, 1997; Chen et al., 1998; Xie et al., 2001; Huang et al., 2002, 2003, 2009; Luo et al., 2003; Wang and Huang, 2008; Yan et al., 2011; Zhang et al., 2013; Sun et al., 2014; Liu et al., 2015b). Current research shows that (1) the detrital age spectrum of the second member of the YGHF in the DF tectonic area is complex,

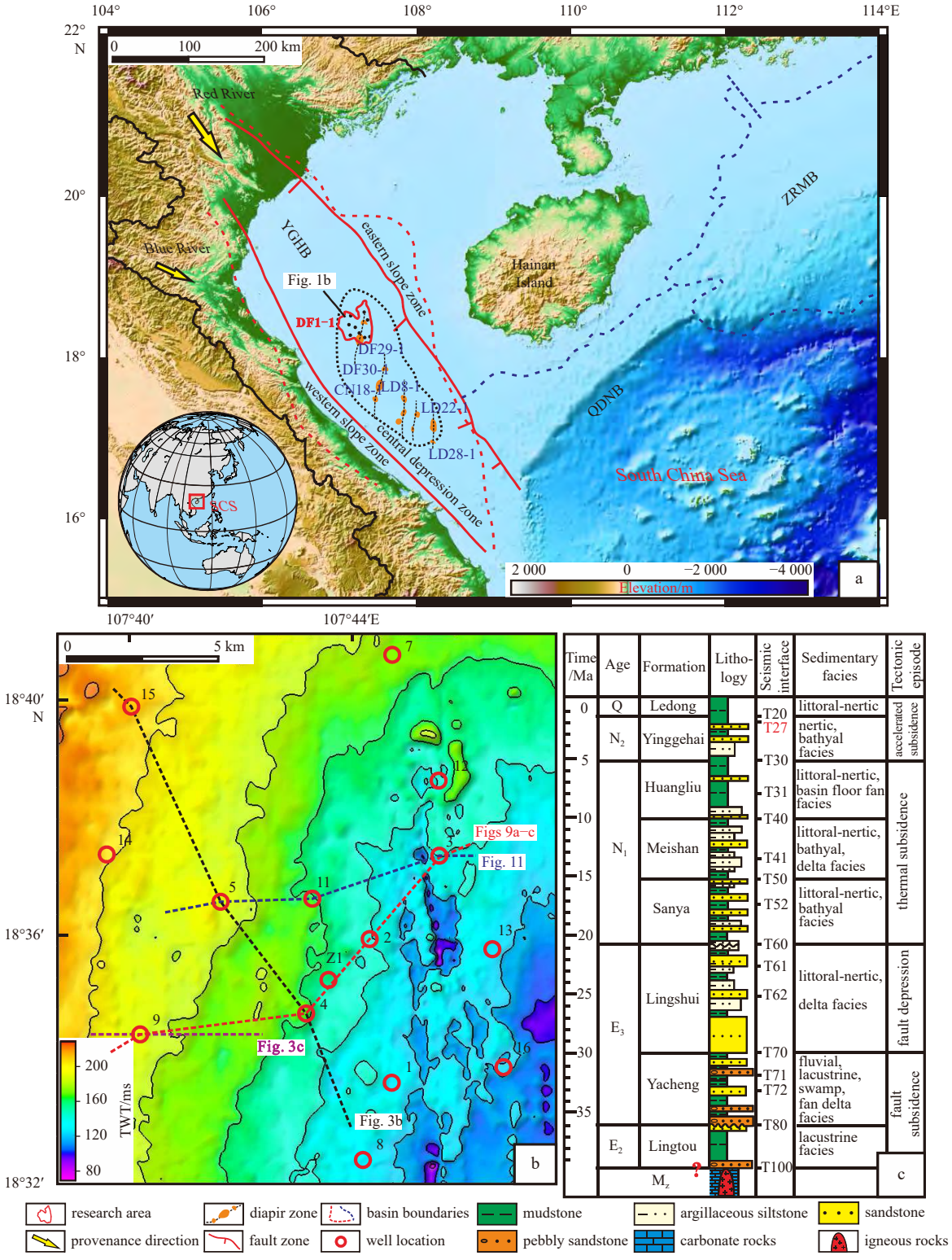

Fig. 1. Regional location and Cenozoic strata comprehensive histogram of the study area. a. Bathymetric map showing the location and geological context of the DF1-1 gas field in the Yinggehai Basin, northwestern margin of South China Sea. b. Time thickness map of the second member of YGHF in the DF1-1 gas field (gas formations I–IIIU), showing a gradually decreasing stratigraphic thickness from northwest to southeast, with an obvious step-like pattern of decline, which also indicates that the provenance of the study area was from the northwest direction during the deposition periods of the four gas formations. c. The comprehensive histogram of stratigraphic and sedimentary facies shows the changes in lithology and sedimentary facies of the sedimentary strata of the YGHB in the northern SCS since the Cenozoic against the background of four major tectonic evolution stages. YGHB: Yinggehai Basin; QDNB: Qiongdongnan Basin; ZRMB: Zhujiang River Mouth Basin; TWT: two-way-travel time; Q: Quaternary; N_1: early Neogene; N_2: late Neogene; E_2: middle Paleogene; E_3: late Paleogene; M_z: Mesozoic basement.

and it is a mixed area dominated by the Red River provenance; (2) the main source rocks are the medium-deep Meishan and Sanya formations, and mature source rocks cover the whole area and dominantly generate gas; the Sanya Formation and Meishan Formation entered the peak period of hydrocarbon expulsion during the depositional periods of the Meishan and Yinggehai formations, respectively, and a small amount of source rocks in the Huangliu and Yinggehai formations also continued to expel hydrocarbons, acting as a sufficient gas source with a short diffusion time, which is conducive to the preservation of natural gas; (3) the shallow-semideep marine siltstones and fine sandstones in the Yinggehai and Huangliu formations, the deep littoral-neritic facies turbidite sand bodies, and the low-level delta sand bodies can act as good reservoirs; (4) the upward arch of mud diapirs in the central depression provides paths for the vertical migration of natural gas. Reservoirs near the source rocks were charged first, and those above them were charged later, forming an episodic pattern of natural gas accumulation, transformation, reaccumulation, and retransformation in the YGHB.

The strata of the YGHF are developed in both the Yinggehai and Qiongdongnan basins. With increasing water depth from northwest to southeast, the sedimentary environment gradually undergoes a transition from the neritic continental shelf of the YGHB to the bathyal continental slope of the QDNB. He et al. (2011), based on the quantitative analysis of foraminifera content in the rock debris of Well 11 in the DF1-1-1 gas field, discussed the evolution of the sedimentary environment since the Miocene. Benthic foraminifera are obviously controlled by the ecological environment, while planktonic foraminifera and calcareous nannofossil zones are highly isochronous and globally comparable (Bolli and Saunders, 1985; Wade, 2004). The paleowater depth is estimated based on the percentage of planktonic foraminifera and the relationship between the percentage of planktonic foraminifera (P) and paleo-water depth (D) in the western SCS established by Li et al. (2004). The results show that the depth of gas formations I–IIIU in Well 11 is approximately 1 289.6 m to 1 437.6 m, which is located in the early stage of VII N21. The paleo-water depth is between 25 m and 45 m, which implies a shallow marine inner continental shelf environment (Fig. 2).

The lithology of the second member of the YGHF in the DF gas field is fine, and the sand bodies are very fine sandstone-coarse siltstone. The sedimentary period of the four gas formations lasted approximately 1.5 Ma to 2 Ma. Vertically, each gas formation is equivalent to a 4th-order sequence with coarsening-upward sediments and a shallow water body (Fig. 3). Each 4th-order sequence corresponds to a small-scale, rapid relative sea level fall, lasting approximately 0.5 Ma. Four 4th-order sequences constitute a 3rd-order sequence. The sequence boundary, i.e., the top surface of gas formation I, is a regional transgressive surface. Large-scale retrogradation reflections and a large set of stable mudstones of overlying gas formation 0 indicate a large-scale relative sea level rise, forming regional unconformity T27 at approximately 2.5 Ma, which is the boundary between the first and second members of the YGHF (Fig. 3).

3 Samples and methods

Poststack time migration-processed high-precision 3D seismic data covering the whole study area were provided by the Research Institute of Zhanjiang Branch, China National Offshore Oil Corporation (CNOOC). The 3D seismic coverage area was approximately 323 km^2, the seismic frequency bandwidth was 15–120 Hz, the dominant frequency of target strata was 45 Hz, and the vertical sampling interval was 2 ms. Drilling and logging data from 14 exploration wells in the study area were collected

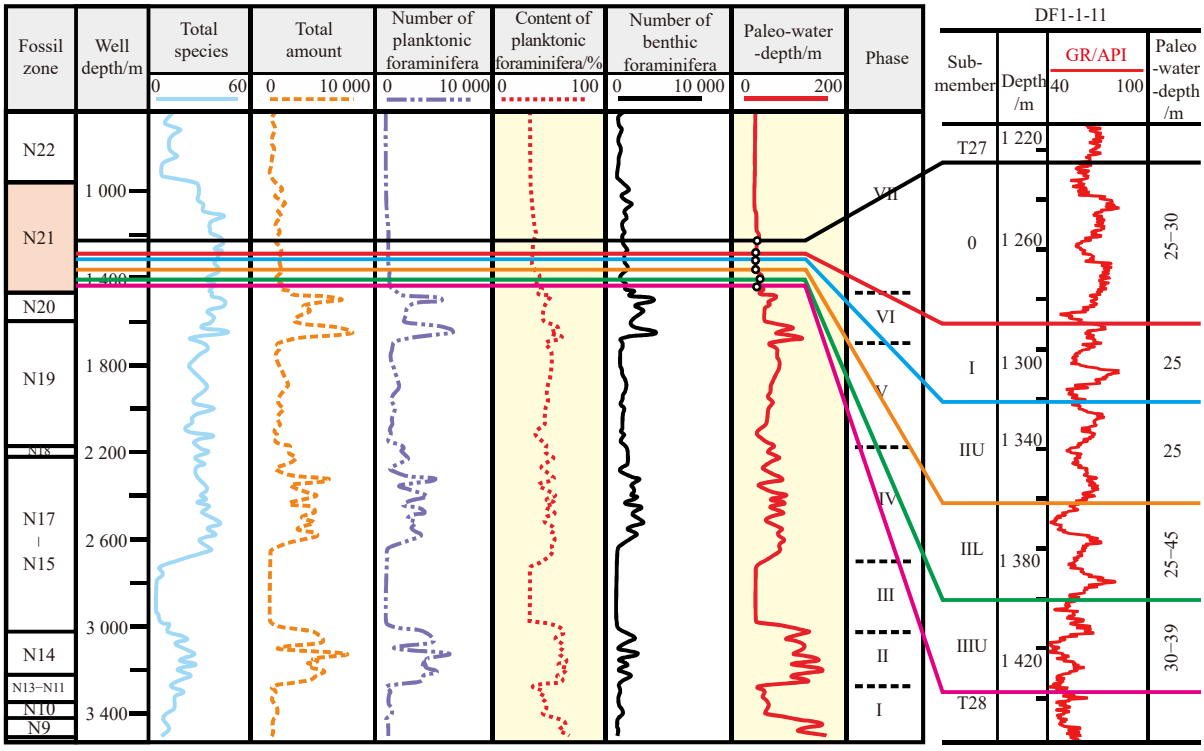

Fig. 2. Content of planktonic foraminifera, paleo-water depth curve and horizon calibration of Well DF1-1-11. The relationship between the percentage of planktonic foraminifera (P, %) and paleobath (D, m) in the western South China Sea is according to Li et al. (2004). The paleo-water depth curve is according to He et al. (2011). Well 11 is located in the middle of the gas field, and its location is shown in Fig. 1b. The results show that gas formations I–IIIU of Well 11 in the DF1-1 gas field correspond to the early stage of the VII N21 zone, and the paleo-water depth is approximately 25–45 m. GR: natural gamma ray.

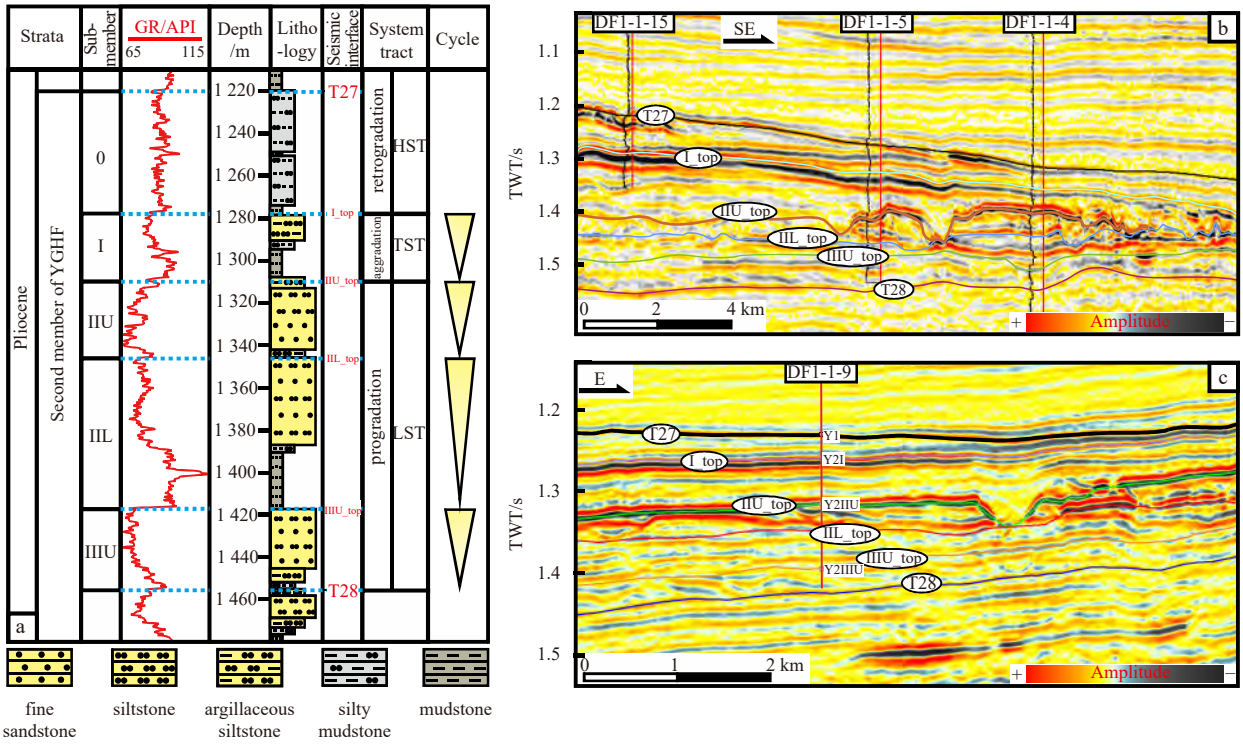

Fig. 3. Typical logging sequence and seismic horizon framework of the second member of the Yinggehai Formation (YGHF) in the Yinggehai Basin (YGHB). a. Sequence division and stratigraphic histogram. b. Seismic cross-section of Wells 15, 5, and 4 in the SE direction. c. Seismic cross-section of Well 9 in the WE direction. See Fig. 1b for the locations. TWT: two-way-travel time; GR: natural gamma ray.

and sorted. Sixty-five cores from 10 wells were observed and photographed in the core database of the Research Institute of Zhanjiang Branch, CNOOC. The total core length was 427.36 m, the recovery rate reached 83.2%, and the core length of the reservoir section was 372.23 m. Several thousand grain size data points on cores from 7 wells, namely, Wells 2, 3, 4, 5, 7, 8 and 9, in the study area were collected, and probabilistic grain size curves and CM diagrams were drawn. Eleven whole-rock sandstone samples were analyzed by X-ray diffraction, and twenty-three sandstone samples were identified by thin-section observations; these samples represented the I–IIIU formations and were analyzed at the State Key Laboratory of Continental Dynamics (Northwest University). After crushing, washing, electromagnetic separation and heavy liquid separation, zircon samples Q3-29, Q5-17 and Q9-01 were obtained from sandstone samples collected from Wells 3, 5 and 9. Each sample contains 100 detrital zircons. LA-ICP-MS detrital zircon U-Pb dating was carried out in the State Key Laboratory of Continental Dynamics (Northwest University), and the age distribution histograms were analyzed and drawn.

Through drilling horizon calibration, the interface of each gas formation was tracked and interpreted on a 3D seismic section. A typical delta progradation reflection and a bottom current erosion channel intersecting with the delta extension direction at a wide angle were identified. The shape, scale, plane distribution and interrelationships of the delta front and bottom currents were determined when combined with the thickness, amplitude and waveform of the progradation bodies and the erosion channels, and a sedimentary model of this area was established according to the analysis of drilling sedimentary facies. By analyzing the origin of high-amplitude bright spots in gas reservoirs and their relationship with diapir structural traps and energy attenuation, the influence of amplitude attribute changes on sedimentary facies analysis was eliminated, providing a basis for reservoir identification and description.

4 Results

4.1 *Lithofacies*

The main lithologies of cores from wells in the study area are very fine sandstone, coarse siltstone, argillaceous siltstone, silty mudstone, and mudstone (Figs 4a–e), and the cores of wells in the west are generally less compacted than those in the east. The logging lithology data show that in gas formations IIIU–IIU, there are large sets of argillaceous siltstone with thin mudstone beds, while in gas formation I, there is a large set of mudstone with thin siltstone beds. The probability particle size curves (Fig. 4f) of Well 9 in the southwestern part, Well 5 in the central part and Well 7 in the northeastern part of the study area are characterized by either “two segments” or “three segments”, which are mainly associated with saltating and suspended transport, with almost no rolling transport. Saltating and suspended components each account for 50% of the total components. The saltating line segment is steeper, while the suspended line segment has a lower slope, and the difference between the two is quite distinct, reflecting the grain size characteristics of traction flow. The thin-section petrological composition and structural maturity analyses show that the sandstone composition and structural maturity are moderately low, indicating rapid deposition. X-ray diffraction whole-rock analysis reveals that the study strata are mainly composed of quartz and feldspar (Table 1) with poor sorting and rounding, implying that during the depositional period of the second member of the YGHF in the DF1-1-1 gas field, sediment was rapidly deposited near the source in a shallow-water environment.

The observation and identification of the typical sedimentary

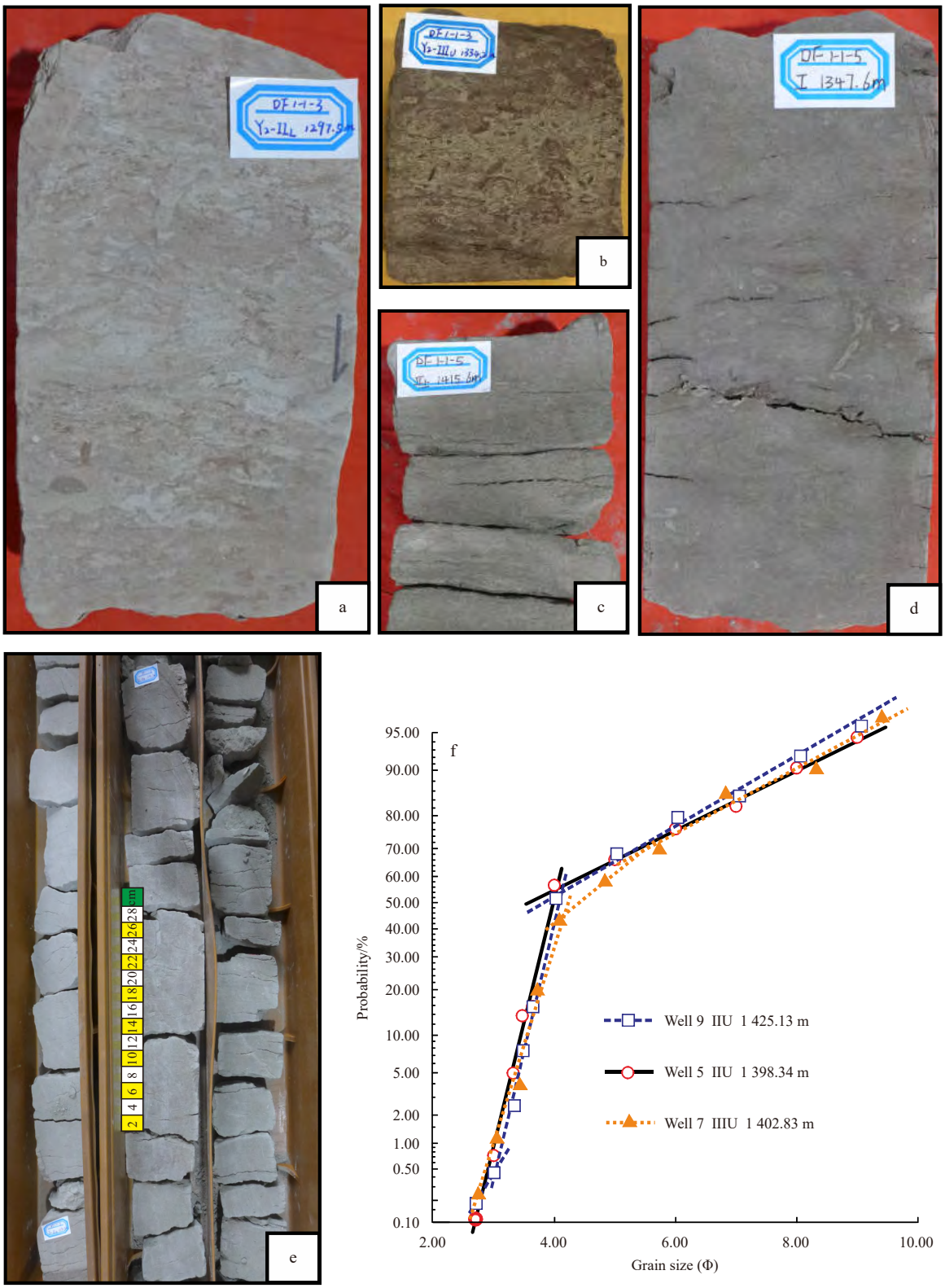

Fig. 4. Lithological characteristics of cores in the second member of Yinggehai Formation in the DF1-1 gas field, Yinggehai Basin. a. Light gray fine siltstone, Well 3 gas formation IIL, 1 297.5 m. b. Reddish brown argillaceous siltstone, Well 3 gas formation IIIU, 1 334.2 m. c. Gray siltstone, Well 5 gas formation IIU, 1 415.6 m. d. Dark gray argillaceous siltstone (containing biological trace fossils), Well 5 gas formation I, 1 347.6 m. e. Argillaceous siltstone in the upper part, siltstone in the middle and lower parts, Well 5 gas formation IIU, 1 390.94–1 395.95 m. f. The probability particle size curves show the traction flow characteristics of "two segments" and "three segments".

structures in the core wells indicate that the main types of sedimentary structures are fine sandstone-siltstone with interlamin-

Table 1. X-ray diffraction whole-rock data of quartz and feldspar content analysis of sandstone samples from the second member of the Yinggehai Formation in the DF1-1 gas field

Sample number	Sampling depth/m	Horizon	Quartz content/%	Feldspar content/%	Quartz content & Feldspar content/%	Ratio of Quartz to Quartz & Feldspar/%	Ratio of Feldspar to Quartz & Feldspar/%	Lithology
2-02	1 359.5	IIIU	56.3	26.4	82.7	68.1	31.9	feldspar sandstone
3-14	1 351.0	IIIU	67.4	23.1	90.5	74.5	25.5	feldspar sandstone
3-26	1 299.5	IIL	60.0	22.6	82.6	72.6	27.4	feldspar sandstone
4-02	1 319.0	IIU	55.4	29.3	84.7	65.4	34.6	feldspar sandstone
5-05	1 433.3	IIU	60.1	27.1	87.2	68.9	31.1	feldspar sandstone
5-22	1 398.2	IIU	62.4	24.8	87.2	71.6	28.4	feldspar sandstone
7-01	1 412.4	IIU	60.2	26.8	87.0	69.2	30.8	feldspar sandstone
7-03	1 367.0	I	67.4	15.4	82.8	81.4	18.6	feldspathic quartz sandstone
8-02	1 461.3	IIIU	61.6	26.4	88.0	70.0	30.0	feldspar sandstone
9-01	1 464.4	IIL	61.1	23.4	84.5	72.3	27.7	feldspar sandstone
9-02	1 428.4	IIU	59.6	25.9	85.5	69.7	30.3	feldspar sandstone

ar fractures, massive argillaceous siltstone with mud clasts, massive siltstone-fine sandstone with mud-coated structure, rhythmic bedding, flaser bedding, convolute bedding, and trace fossils (biological burrows) (Fig. 5).

4.2 *Logging facies*

The logging response characteristics of representative Wells 3 and 5 in the eastern and western parts are shown in Figs 6 and 7, and the analysis of the data shows that the western wells in the study area represented by DF1-1-5 mainly feature parasequence-related funnel-shaped logging facies with multiple consecutive reverse cycles (Fig. 6). The parasequence-related logging facies indicates a shallow subaqueous environment, while the reverse-cycle funnel-shaped facies reflects overflowing bank sedimentary microfacies with enhanced upward flow energy and better sorting, typically associated with a delta front mouth bar, front sand bar, etc. DF1-1-3 in the east features strongly toothed bell-shaped or toothed funnel-shaped logging facies (Fig. 7). The strong toothing represents intermittent depositional superposition and turbulent water, which characterizes rapid near-source deposition, and the bell-shaped lithology is mainly associated with a normally graded grain size sequence, which is a sedimentary characteristic of distributary channels.

A summary of the logging facies analysis of each gas formation in the exploration wells in the study area shows that gas formations IIU–IIIU in Wells 5, 8 and 9 in the west are mainly parasequence-related funnel-shaped and low funnel-shaped logging facies, while in Wells 2, 3 and 4 in the east, they are mainly toothed bell-shaped or toothed funnel-shaped logging facies. Gas formation I features mostly parasequence-related logging facies, including the parasequence-related moderately to strongly funnel-shaped type and the parasequence-related top transitional type. Based on these observations and the typical sedimentary structure characteristics observed in the cores, a shallow sea delta depositional system was present during the sedimentary period of the second member of the YGHF in DF1-1.

4.3 *Seismic facies*

Based on the 3D seismic data from the DF1-1-1 gas field, a total of 7 seismic facies types have been identified in the second member of the YGHF (Fig. 8): A. medium-amplitude retrogradation reflection, B. high-amplitude wedge reflection, C. medium-amplitude parallel sheet reflection, D. progradation reflection, E. low-frequency parallel-subparallel blank reflection, F. extremely low-frequency mound-like blank reflection and G. channel filling (progradation filling, bilateral onlap filling and blank filling). The most important seismic facies are D and G.

In the seismic section, obvious differences appear in the seismic reflection amplitude and frequency of each gas formation from east to west in the second member of the YGHF (Fig. 3b). In the western part of the study area, seismic reflections feature high frequency, medium-low amplitude and strong continuity. Progradation reflection structures are typical and can be easily identified in this section. In the eastern diapir region, the reflection structure of the seismic facies is gradually transformed into a low-frequency, high-amplitude and weak-continuity structure influenced by the diapir and gas, which is similar to the "parallel sheet" seismic facies in shape, and the dominant frequency also decreases from 45 Hz to approximately 40 Hz.

5 Discussion

5.1 *Genesis of high-amplitude seismic reflections*

After horizon T27 is flattened, the seismic section, sedimentary facies section and attenuation anomaly section of Wells 9, 4, 2, and 3 in the NE direction are constructed, as shown in Figs 9a–c, and the plane positions can be seen in Figs 1b and 10 *AA′*. Figure 9a shows that the amplitude energy of seismic reflections is obviously different between the east and the west. The gas formations IIIU and IIL are the most typical; the closer to the eastern part of the study area, the more the profiles show the characteristics of low-frequency, high-amplitude and strong-continuity reflections. The amplitude variation reflects the lateral variation in the wave impedance difference at a specific interface, and the frequency variation is often related to the spacing of the reflection interfaces and the changes in strata velocity (Sheriff and Geldart, 1995). Frequency attenuation is generally caused by low velocities, which in turn generally result from gas-bearing or special lithologies (Brouwer et al., 2008; Zeng, 2010). Gas reservoirs are characterized by "low-frequency shadow" and "high-frequency attenuation" (Chen and Jeng, 2011; Lu et al., 2013; Carcione et al., 2018). It is well established that seismic waves passing through gas-bearing strata in this area have very high amplitudes and significant attenuation (Goloshubin and Bakulin, 1998; Hedlin et al., 2001; Castagna et al., 2003; He et al., 2008). The generalized low-frequency shadow gas-bearing detection method used in this study is based on the above principle. The color scale of the anomaly profile shows yellow and red as high values of attenuation anomalies, purple and blue as low values, and light blue as the background value (Fig. 9c), and the attenuation anomaly value is dimensionless. Drill cores from Wells 9, 4, 2, and 3 confirm that the gas-bearing layers correspond well to the high-value zone of the attenuation anomaly and that the method is applicable to the study area.

Both gas formations IIIU and IIU in Well 9 have obvious progradation reflections, with IIU having high amplitude and IIIU

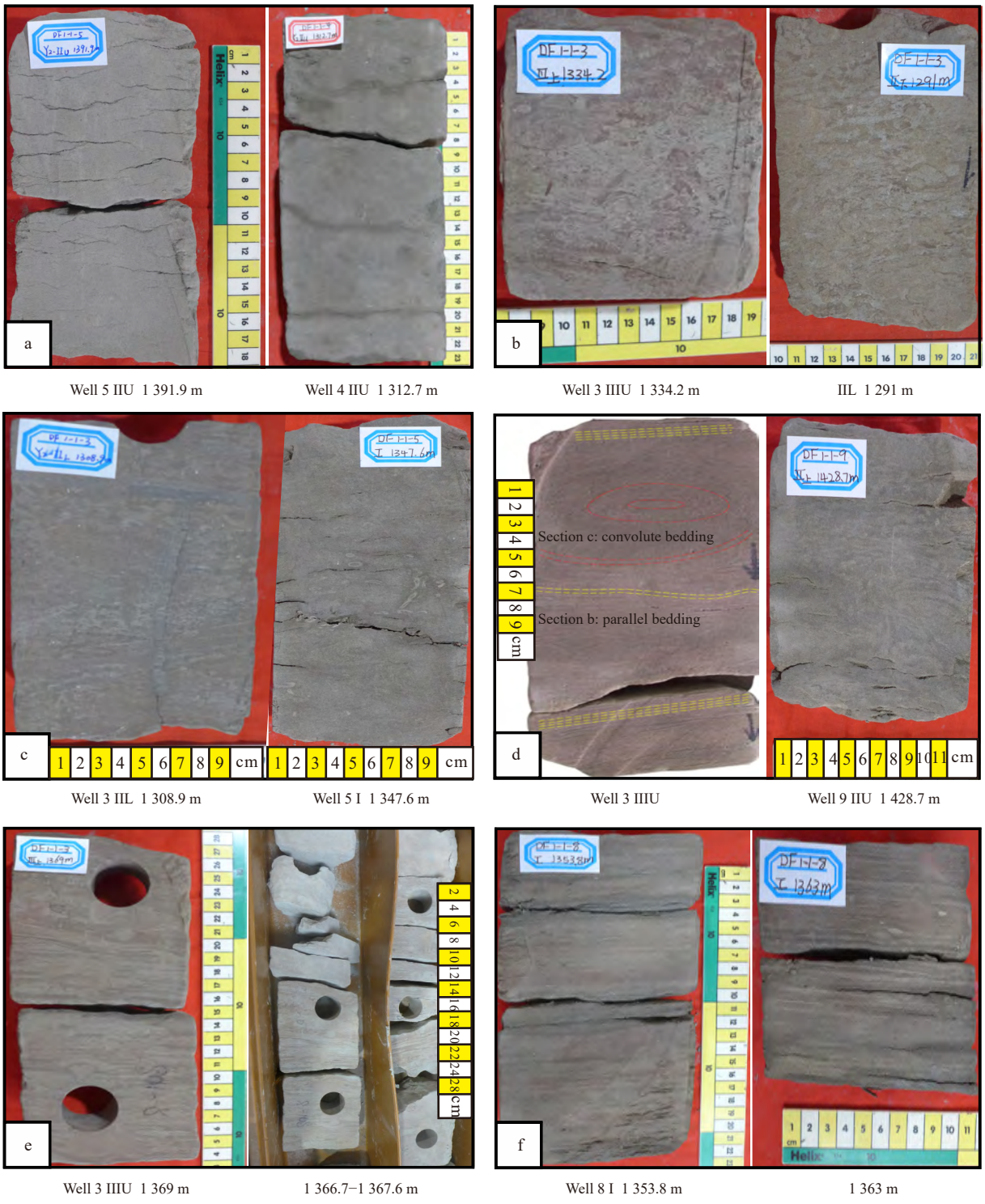

Fig. 5. Sedimentary structure types of the second member of Yinggehai Formation in the DF1-1 gas field, Yinggehai Basin. a. Fine sandstone-siltstone with interlaminar fractures. b. Massive argillaceous siltstone with mud clasts, where a large number of biological disturbance occur. c. Massive siltstone with biological burrows. d. Shallow sea storm sedimentary sequence, with Section b showing parallel bedding in the lower part and Section c showing convolute bedding in the upper part. e. Rhythmic bedding. f. Flaser bedding.

having medium-low amplitude (Fig. 9a). Drilling results indicate that gas formation IIIU encountered an 18.3 m-thick water layer and that gas formation IIU encountered two sets of sandstone layers with a total thickness of 23.8 m, the top of which bears gas (Fig. 9b). The gas-bearing detection anomaly profile also shows that the attenuation value (dimensionless) of gas formation IIU is significantly higher than that of gas formation IIIU in Well 9 (Fig. 9c). In addition, gas formations IIU and IIL in Well 4 and gas formations IIL and IIIU in Wells 2 and 3 are all in thick gas layers (Fig. 9b), which is consistent with the high-amplitude area in Fig. 9a and the high values of attenuation in Fig. 9c. These features suggest that both strong and weak reflections can represent sandstones, with mudstones producing weak reflections, water-bearing sandstones having medium-amplitude reflections, and

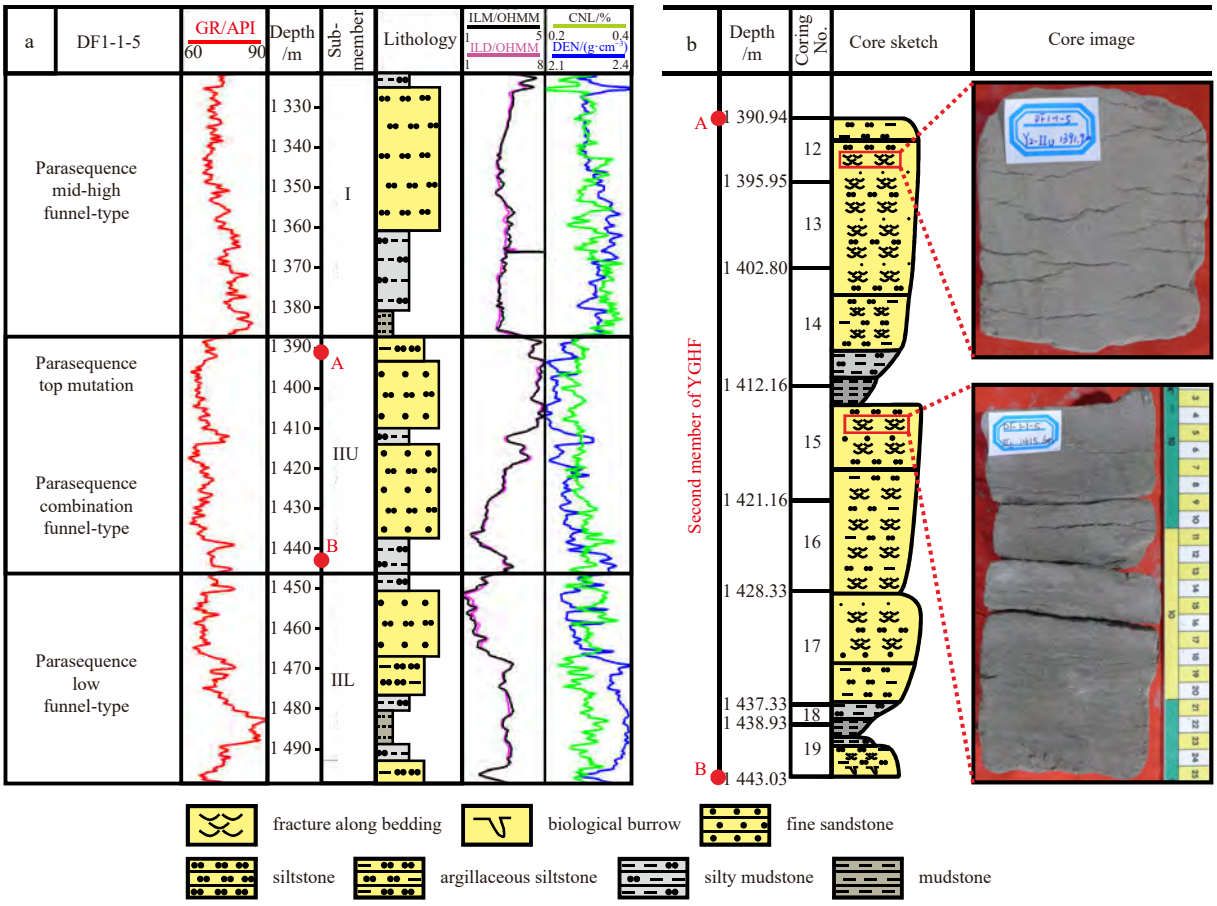

Fig. 6. Logging facies type (a) and core sketch (b) of the second member of the Yinggehai Formation (YGHF) in representative Well 5 in the western part of the DF1-1 gas field. Several reverse cycle parasequence-related logging facies types are mainly developed, and a large number of interlaminar fractures are developed in fine sandstone-siltstone cores. GR: natural gamma ray; ILM: resistivity of medium investigated induction log; ILD: resistivity of deep investigated induction log; CNL: compensated neutron log; DEN: density log.

gas-bearing sandstones showing high amplitudes.

The above results indicate that the second member of the YGHF in the DF gas field is a bright spot-type gas reservoir, and the low frequencies and high amplitudes in the eastern part of the study area indicate that the sandstones contain gas. The whole gas formation IIIU belongs to a set of progradation body reflections, and the seismic resolution cannot present the complete progradation features due to the widening of the seismic event of gas-bearing attenuation toward the east (Fig. 9a). Drilling also revealed that the gas-bearing degree of sandstone in the high-amplitude "parallel reflection" seismic facies is better than those of other seismic facies and that all the other gas formations have similar characteristics.

The top of the delta system in gas formation IIU was strongly eroded by bottom currents after deposition, and the thickness of the reformed delta front sand body varies widely from 0 m to 60 m. The reservoir porosity ranges from 20% to 33%, and the permeability ranges from 20 mD to 517 mD, which implies a medium-porosity and medium-permeability reservoir. The top surface structure, thickness, root mean square (RMS) amplitude and energy attenuation maps of gas formation IIU in the time domain are shown in Figs 10a–d. The top surface structure and thickness map clearly illustrates that the whole gas formation IIU is low in the northwest and high in the southeast (Fig. 10a). The strata in the west are thick, and those in the east are missing across a large area (Fig. 10b). The high values of the RMS amplitude are distributed in a circular pattern in the eastern and southern parts of the study area, the amplitude values are generally greater than 4 (dimensionless), and the two-way travel time is less than 1 300 ms. The bright spot range is basically consistent with the tectonic pattern of a dome anticline (Fig. 10c). The generalized low-frequency shadow method is used to obtain the abnormal plane map of gas-bearing attenuation (Fig. 10d). On the color scale, dark red marks abnormally high values of attenuation, black represents low values, and white shows the critical value. Attenuation values greater than 10 indicate the possible gas area, i.e., the red range in the figure. Comparing the anomalous range in Fig. 10d with the top surface structure and the high value area of the RMS amplitude attribute clearly reveals that the high-amplitude area is basically located at the high point of the structure and may bear gas.

The aforementioned results confirm that the RMS amplitude in this area does not reflect information about sedimentary facies but indicates the gas-bearing range, which cannot be used to determine the distribution of facies. The distribution of gas reservoirs in this area is obviously controlled by tectonics, and the sand bodies in this area are well developed and are mainly located in the high part of the dome-shaped diapir zone and its periphery. The mudstone interlayer is well sealed, and the faults generated by diapir uplift caused no obvious loss in the gas reservoir; hydrocarbons are still in the processes of expulsion, migration and accumulation.

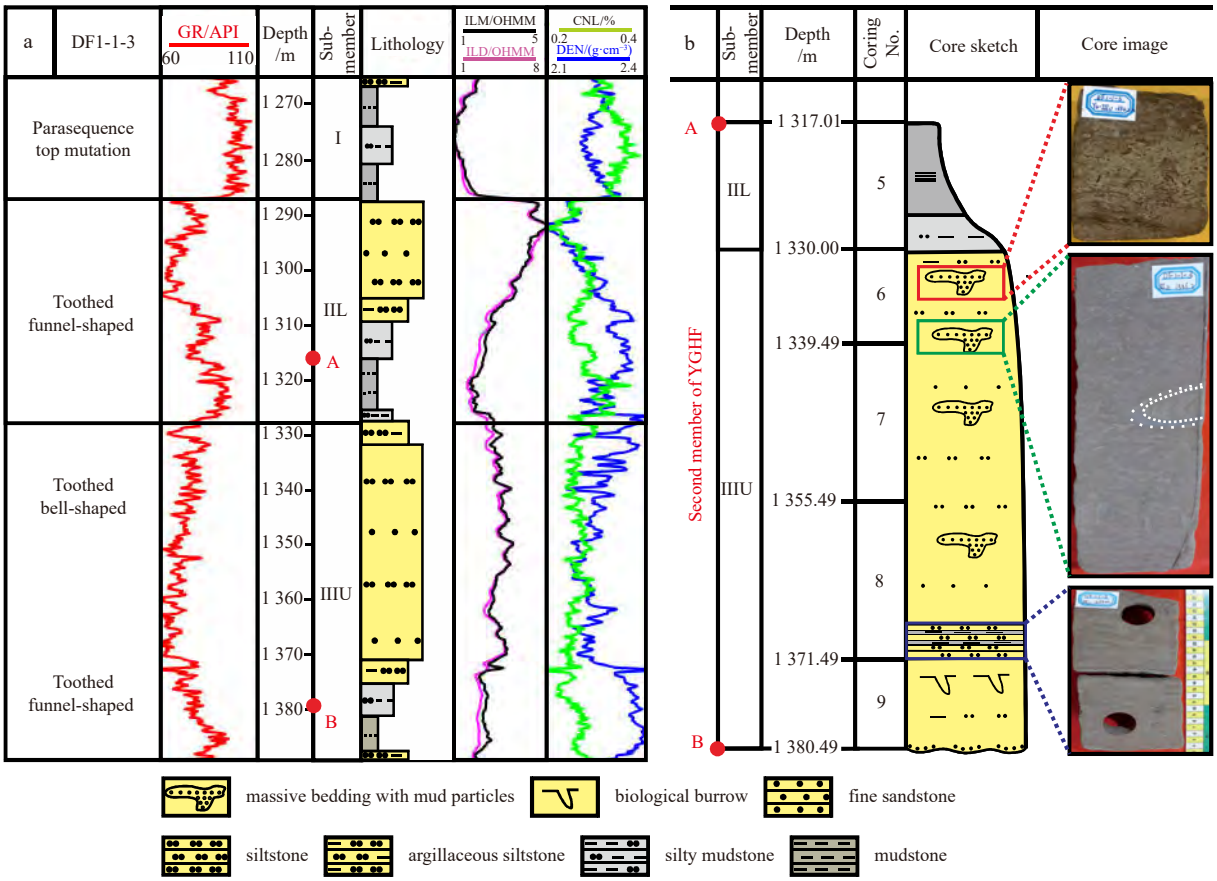

Fig. 7. Logging facies type (a) and core sketch (b) of the second member of the Yinggehai Formation (YGHF) in representative Well 3 in the eastern part of the DF1-1 gas field. Several parasequence-related toothed bell-shaped or toothed funnel-shaped logging facies are mainly developed. Cores contain mud clasts, and a large number of biological disturbance characteristics can be seen. GR: natural gamma ray; ILM: resistivity of medium investigated induction log; ILD: resistivity of deep investigated induction log; CNL: compensated neutron log; DEN: density log.

5.2 *Relationship between delta front and bottom current erosion channel filling*

5.2.1 *Filling of bottom current erosion channel*

Li et al. (2010) proposed that the DF1-1-1 gas field is generally located in the transition zone between nearshore and offshore environments. Sediments with loose grains and high argillaceous content slide, triggered by a certain mechanism, and gravity flow erosion channels are well developed in the study area, which are called mud flow gullies. The interiors of these gullies are filled mainly with mudstone and can be clustered and distributed in patches in the gentle topography and form lateral and vertical barriers that affect sand body connectivity. In this study, based on the analysis of the plane shape, fill characteristics, grain size data and paleoenvironment of this kind of erosion channel, we consider that these channels are surface bottom current channels developed in a shallow marine environment.

Bottom currents have a wide range of types, including bottom currents generated by temperature-salinity differences, wind-driven circulation, gulf currents, internal waves and internal tides. Among these types of currents, those parallel to the continental slope strike are called "contour currents" (Shanmugam, 2000, 2003). Stow et al. (2002) classified bottom currents into deep (>1 500 m), intermediate and surface (<350 m) currents according to the water depth at which they developed. Deposition as a result of interactions between bottom currents and gravity flows occurs widely in deep-water environments (Schopf, 1981; Faugères and Stow, 1993; Massé et al., 1998; Faugères et al., 1999; Chen et al., 2016). The sediments in the first two depth zones are transported and deposited by contour currents in a normal deep-water environment, while the distribution of sedimentary sand bodies under shallow surface bottom currents is more susceptible to the effects of Earth's rotation and hydrodynamic factors such as monsoons, tides, waves, internal waves, and eddies (Viana et al., 1998).

The water circulation in the northern SCS is complex, with deep currents flowing clockwise in the SSW direction and intermediate currents flowing counterclockwise along the slope in the SSE direction (Qu and Lindstrom, 2004; Wang and Li, 2009; Xu et al., 2014). The depth limit of the intermediate current in the SCS is still controversial, with the upper boundary mainly at 300–500 m below sea level (Lüdmann et al., 2005; Zhao et al., 2009) and the lower boundary concentrated at 1 000–1 500 m (Zhu et al., 2010; Chen et al., 2016). Modern surface currents are influenced by the East Asian monsoon, forming a monsoonal circulation with seasonal inversion, flowing clockwise in summer and counterclockwise in winter (Shao et al., 2007).

Multistage bottom current deposits have developed in the northern SCS since the late depositional period of the early Miocene to middle Miocene Meishan Formation. Many contourites have been confirmed in the ZRMB (Zheng and Yan, 2012; Zheng et al., 2016). Recent studies in the southeastern QDNB have also identified drift deposits (Li et al., 2013; Sun et al., 2017), contourite mounds (Tian et al., 2015) and other bottom current sedi-

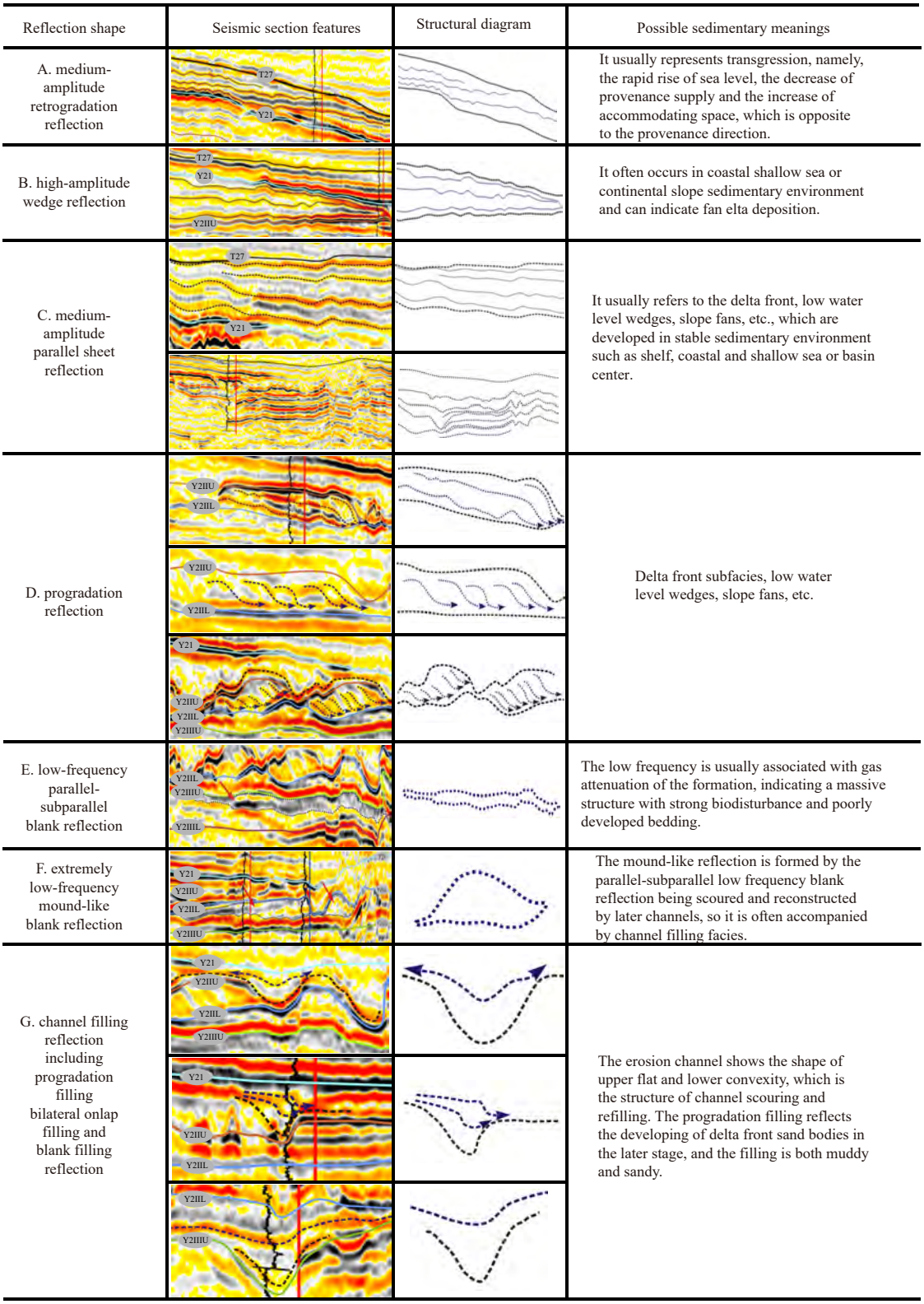

Fig. 8. Typical seismic facies types and possible geological genesis of the second member of the Yinggehai Formation in the DF1-1 gas field 3D seismic survey.

ments. In contrast, bottom current deposits in the YGHB, which are also located in the western part of the northern SCS, have rarely been reported (Chen et al., 2014). The YGHB is situated in the shallow-water area of the northern SCS and is subvertically connected with the QDNB. Although the SCS basin is a confined basin, the YGHB and QDNB underwent similar tectonic evolutionary stages (Ren et al., 2013) during the Cenozoic, with similar sedimentary characteristics and smooth water circulation. In the modern SCS, the sea level rose dramatically after the last ice age, and the surface current system was greatly enhanced, develop-

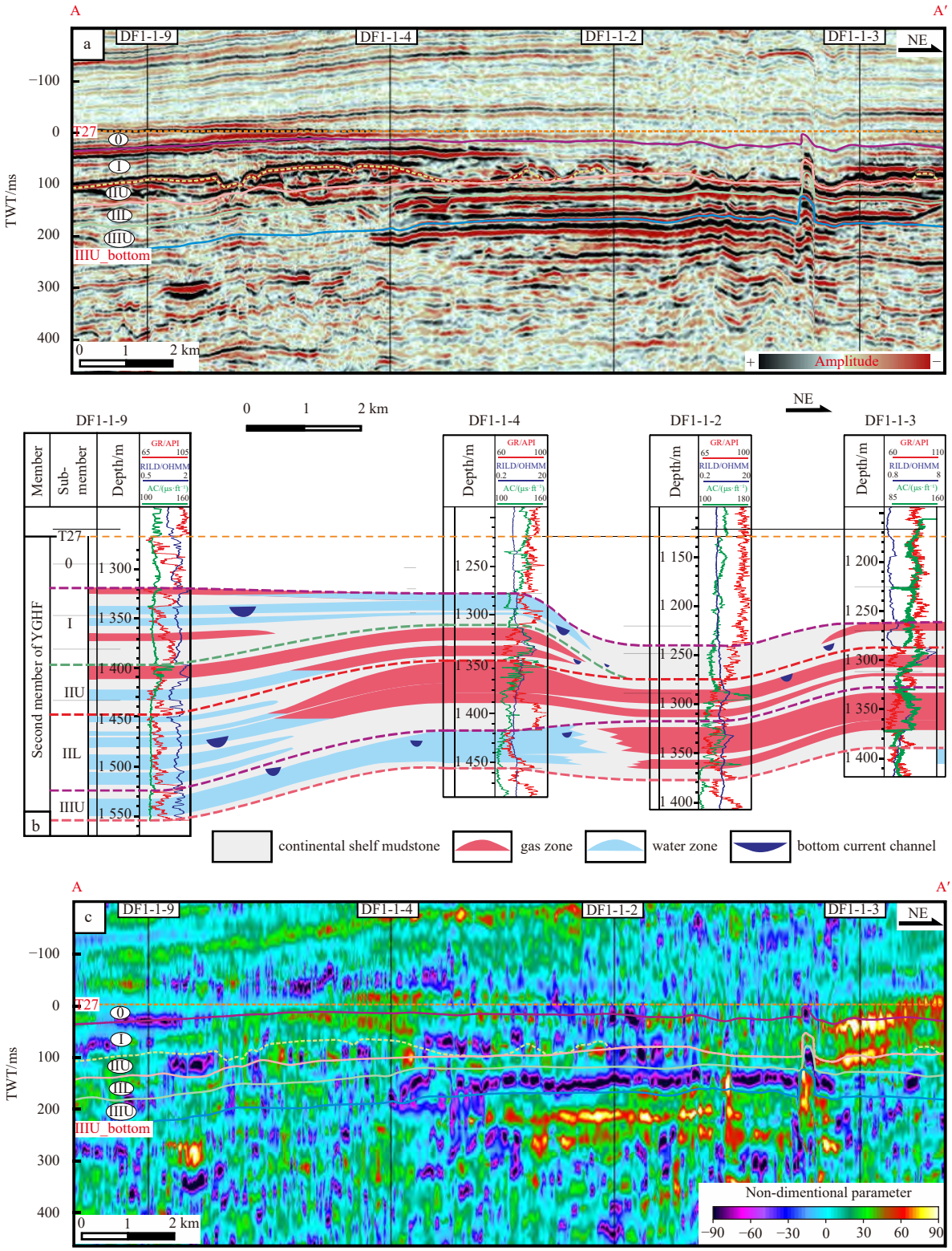

Fig. 9. Seismic sections (a), sedimentary facies (b) and attenuation anomaly (c) of Wells 9, 4, 2, and 3 in the NE direction in the second member of the Yinggehai Formation (YGHF) in the DF1-1 gas field 3D seismic survey. See Fig. 10 AA′ for the location. GR: natural gamma ray; RILD: resistivity of deep investigated induction log; AC: acoustic.

ing a series of systems, including coastal currents driven by rivers entering, SCS warm currents, Kuroshio SCS tributaries, and drift currents influenced by monsoon and geostrophic deflection forces (Liu et al., 2015a; Zheng et al., 2016). In the early Pliocene, the second member of the YGHF was deposited in the interglacial period before the Quaternary glacial period, which was similar to the sedimentary environment of the modern SCS, and the relative sea level height was the highest in the last 10 Ma; this setting produced an active period for the development of bottom currents. The YGHB has geological conditions conducive to the

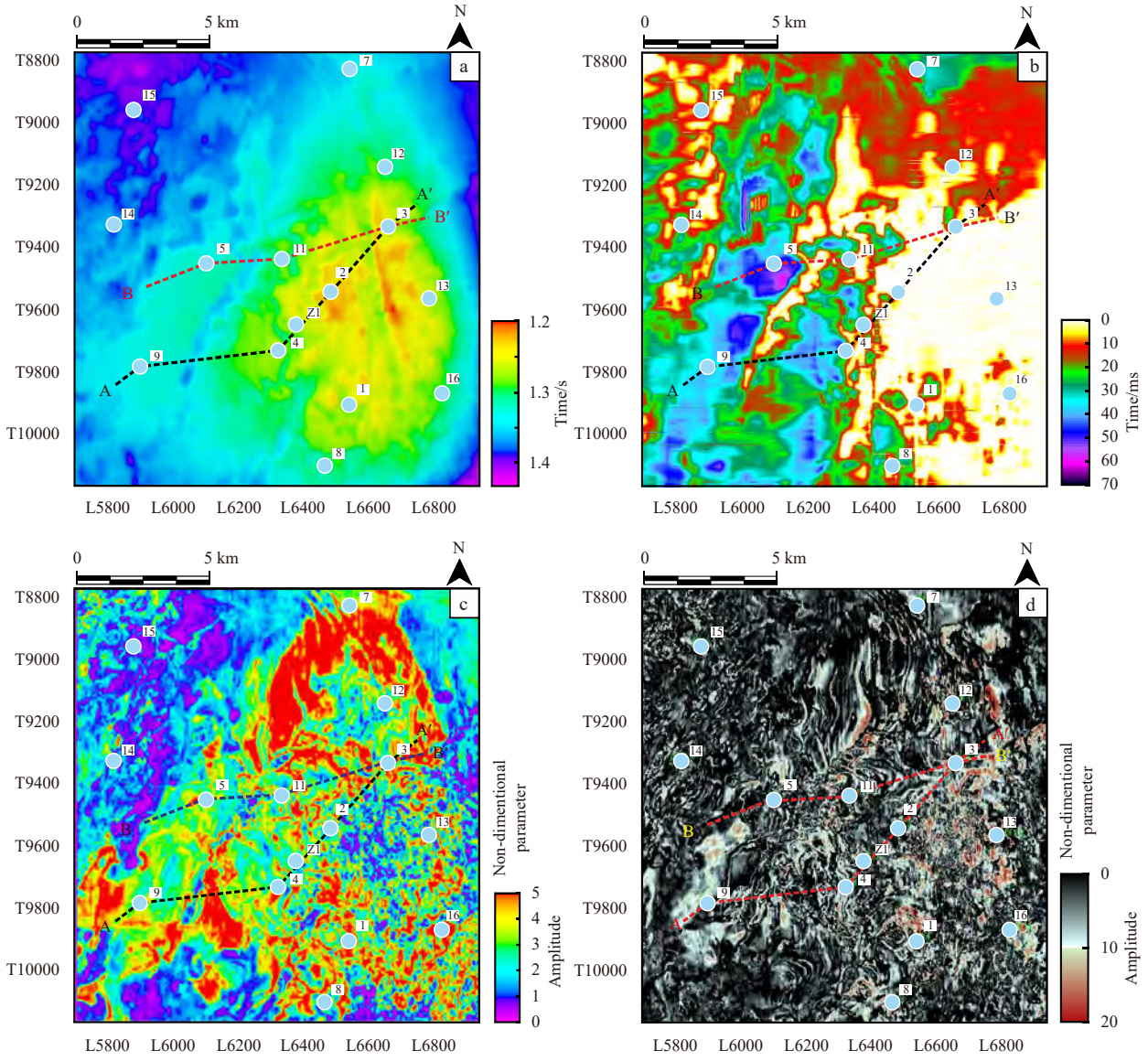

Fig. 10. Plane distribution maps of the top surface structure in the time domain (a), time thickness (b), root mean square (RMS) amplitude (c) and generalized low-frequency shadow attenuation (d) of gas formation IIU in the DF1-1 gas field. See Fig. 9 for profile AA′ and Fig. 11 for profile BB′. L on the *x*-axis means Line; T on the *y*-axis means Trace.

development of surface bottom currents.

At present, there are many reports about the interaction between bottom currents and gravity flows in continental slopes and deep water environments (Wei et al., 2015; Gong et al., 2016b; Fonnesu et al., 2020; Luan et al., 2021). Gong et al. (2016a) studied the drilling cores of the Miocene Zhujiang Formation in the Zhujiang River Mouth Basin of the northern SCS and proposed the identification characteristics of turbidites reworked by bottom currents, that is, the discontinuity of the "Bauma sequence" caused by scattered traction structures and tidal bedding combinations. Fonnesu et al. (2020) studied the offshore Coral and Mamba superlarge gas field reservoirs in the northern Mozambique, which are composed of pure sandstone deposited by large-scale turbidity flow and bottom current, forming asymmetric drift mounds and unidirectional low-angle superposition of channel and lobe complexes. Luan et al. (2021) believed that the development of asymmetric levees in the Pliocene channel-levee-lobe complex deep-water system of the Rovuma Basin in East Africa is the result of the transformation of gravity flow on the western slope by the north-south bottom current, and the formation of high-quality reservoirs is related to the bottom current transformation.

The transformation of shallow-water bottom currents is rarely reported, and research on their interaction with delta sand bodies is still in its infancy.

The depositional period of the second member of the YGHF in the DF gas field was a shallow marine continental shelf environment with shallow water bodies and a gentle and long shelf. Almost no gravity flow deposition occurred, and the provenance was mainly provided by delta traction currents from the NW direction. Similar to modern surface currents (Shao et al., 2007), shallow bottom currents formed by monsoons, Earth surface rotation and other factors flowed clockwise in summer and counterclockwise in winter and cut and formed erosion channels along the shelf (Sun et al., 2016), while delta front deposits developed along the shelf and filled the erosion channels. Superimposed interactions can occur at the same time and at the same location when the two processes are comparable in energy (Gong

et al., 2016a, 2018; Wang et al., 2018), which is consistent with this study. The probability cumulative grain size curves of the bottom currents all have "two-stage" or "three-stage" traction flow features, not "mudflow gullies" of gravity flow genesis. The time interval between the cutting of the bottom current channel and the filling of the delta front at the later stage is very short, and the channel can even be filled while it is cut. The internal fills are not only muddy and sandy sediments but also sandy and muddy interbedded sediments; i.e., there is not a simple muddy channel. For example, the drilling of both gas formation IIIU in Well 4 and gas formation I in Well 2 reveals this bottom current channel (Fig. 9a), with the former containing argillaceous siltstones and the latter mudstones. The type of fill within the erosion channel depends on whether the later sediments supply delta front sand bodies or predeltaic-shallow marine mud.

Due to the lack of reservoir-forming conditions in the negative topography of the channel, high-amplitude fills are relatively rare in seismic sections. The sandy fill mostly shows medium- to low-amplitude progradational filling in the study area, where the medium amplitude reflects the difference in wave impedance caused by lithological changes in the sand-mud interlayers. In contrast, the argillaceous fill is mostly a low-amplitude blank reflection (Fig. 8G), which may reflect a change in the delta channel or the weakening of the source supply, and the extent of sand bodies decreases. The bottom current channel is not as sand rich as the delta front facies and cannot be used as a high-quality reservoir and favorable target zone.

5.2.2 *Delta front reshaped by bottom currents*

The evolution of delta front sand bodies in the seismic cross-sections of Wells 5, 11, and 3 in the NE direction is analyzed by using the balanced profile method, and Figs 11a–d is obtained by flattening the top interfaces of gas formations IIIU, IIL, IIU and I. The results show obvious progradational reflection features (corresponding to delta front sand bodies) for each gas formation in the study area from west to east, reflecting the characteristics of sediments entering the open and gently sloping environment and starting to unload and accumulate toward the sea side (Figs 11a, b). The gas formations IIIU–IIL correspond to two sets of progradational bodies from bottom to top, and the sand body thickness of gas formation IIIU is relatively stable, with an average thickness of 40 ms. The overall thickness of gas formation IIL is thinner, and there is no obvious mudstone interlayer between the IIU and IIL gas layers. The average thickness is less than 30 ms. The lateral extent of the two sets of sand bodies can reach 15 km.

In the early sedimentary stage of the IIU gas formation, many progradational reflection seismic facies developed in Well 5 in the western study area, with a sand body thickness of approximately 25–40 ms and a length of approximately 8.2 km. From the late stage of IIU to the early stage of gas formation I, numerous channel fill seismic facies developed, and the thickness of the

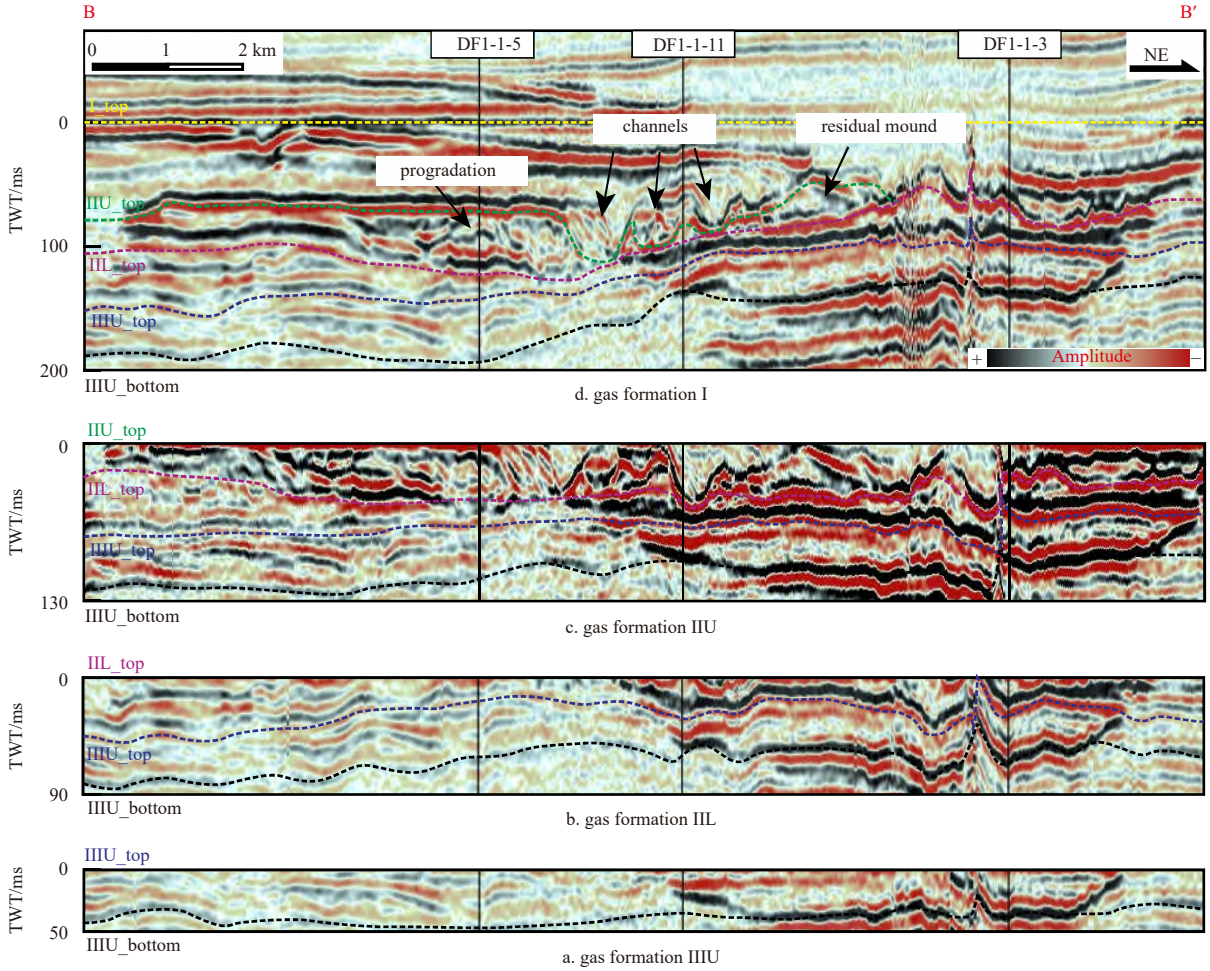

Fig. 11. Seismic facies evolution analysis of the second member of the Yinggehai Formation in the cross-sections of Wells 5, 11, and 3 in the NE direction by flattening the top interfaces. a–d correspond to each deposition period of gas formations IIIU–I. See Fig. 10 BB′ for the profile position.

single fill channel between Wells 5 and 11 reached 40 ms; this channel scoured all the original strata of gas formation IIU. The strong transformation caused the residual progradational bodies to become mound-like and isolated. Gas formation IIU thinned and gradually pinched out near Well 3 in the east (Fig. 11c). The interaction between a delta front and a bottom current is a process of growth and decline (Li et al., 2021). Under certain trigger mechanisms, the depositional energy of gravity or traction flow events is much larger than that of bottom current deposition (Mulder et al., 2006, 2008). The three large bottom current channels in the late IIU gas formation indicate that the relative sea level rose, the provenance supply of delta front sand bodies weakened, coarse clastic injection decreased, and bottom currents developed and dominated. Compared with gas formations IIIU–IIL, gas formation IIU contains sand bodies with an obviously decreased distribution range and is mainly developed in the western part near the provenance area.

The stratigraphic thickness increased significantly during the depositional period of gas formation I, with a maximum of more than 100 ms, and this formation can be roughly divided into two parts: the early progradational body and the late retrogradational body. In the early stage, many bottom current channels developed and were rapidly filled by the progradational body, with a lateral distribution of up to 12 km. In the late stage, the late retrogradational sand body is thinner, and the reflection characteristics indicate that during this period, the relative sea level rose, the provenance supply was weakened or the delta was diverted, the sand body retreated toward the shore, and the lateral distribution was shortened to approximately 8.5 km (Fig. 11d).

5.2.3 *Distribution of reservoir facies*

As noted in Section 5.1, the study area is a typical bright spot gas reservoir, and the high amplitude is caused by gas-bearing sandstone, which does not directly reflect information about sedimentary facies. Studying the distribution of sedimentary facies by using conventional amplitude extraction methods is very difficult (Fig. 10c). How can interference be eliminated to study the distribution and coupling relationships of various sedimentary types in the second member of the YGHF? To solve this problem, we select gas formation IIU, which was most strongly eroded by bottom currents, as an example for analysis.

In the seismic horizon interpretation, the bottom current channel across the whole region is interpreted along the erosion surface at the bottom of the channel. At this time, a comprehensive analysis of the thickness map (Fig. 10b), top structure map (Fig. 10a) and seismic facies plane distribution map (Fig. 12a) can well depict the shape and distribution of the bottom current channel in the late sedimentary stage of gas formation IIU and compensate for the deficiency of amplitude analysis in identifying the sedimentary facies of bright spot gas reservoirs.

The distribution of the bottom current channel is described based on the top surface structure, stratigraphic thickness and seismic facies distribution map, and according to the characteristics of the gamma ray (GR) logging curve of Wells 9 and 4 in Fig. 9b, which shows the top transition of the parasequence, the residual progradational body of the IIU gas formation can be determined to represent a delta front sand body. The combination of this information with the types of seismic facies identified in Section 4.3 allows delineation of the distribution range of pro-

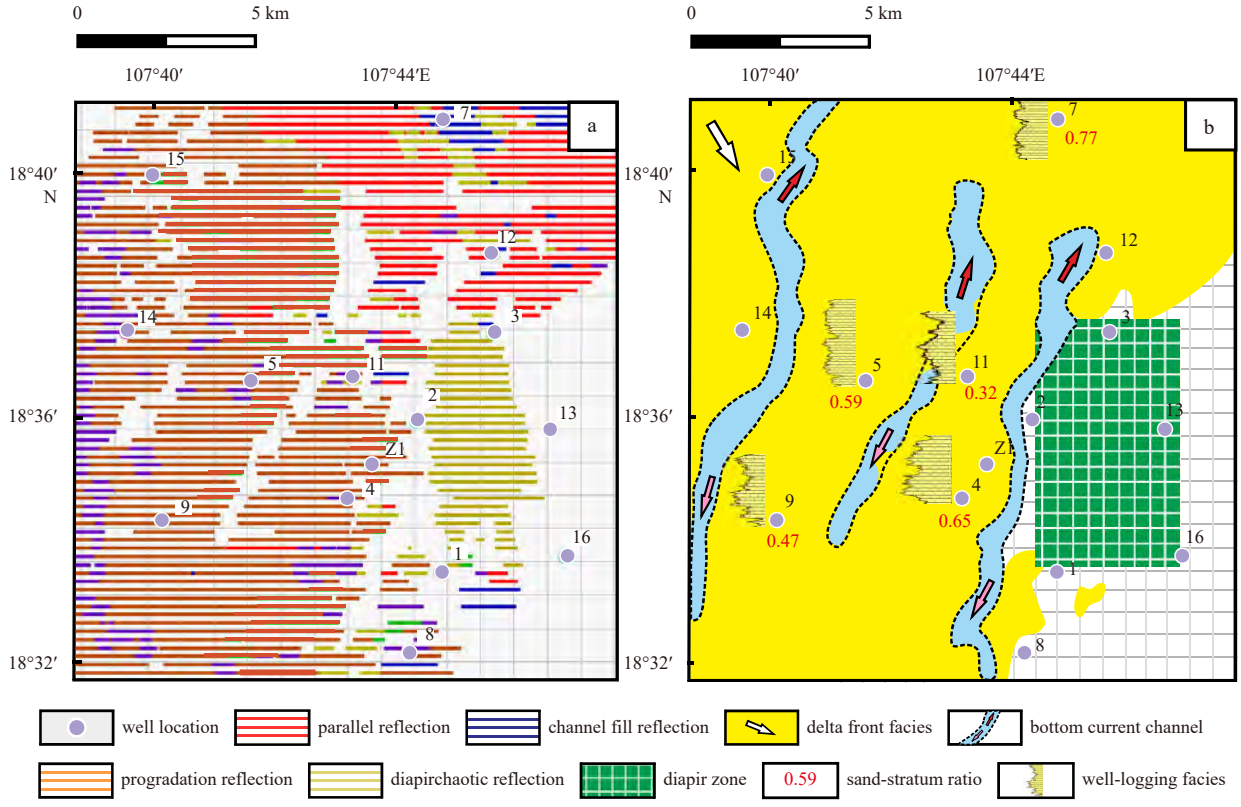

Fig. 12. Plane distribution characteristics of delta front sand bodies and bottom current erosion channels of gas formation IIU in the second member of the Yinggehai Formation in the DF1-1 gas field, Yinggehai Basin. a. Plane distribution map of seismic facies. b. Plane distribution map of sedimentary subfacies. It is inferred that the cause of the shallow-water bottom current is similar to that of the modern surface current. The flow direction is affected by the East Asian monsoon, the red arrow is clockwise in summer and the pink arrow is counterclockwise in winter.

gradational reflection and parallel reflection seismic facies of gas formation IIIU (Fig. 12a); then, the range of the delta front is determined, and the plane distribution map of sedimentary facies of gas formation IIIU is drawn (Fig. 12b).

As illustrated in the figure below, the sand bodies in the delta front are fan shaped, and the lateral sizes of the sand bodies are between 8 km and 15 km. The sand content in the western part of the study area is high, and the seismic section shows a residual progradational reflection caused by the bottom current channel reconstruction (Fig. 9a), while the northeastern stratum has a high mud content, showing a parallel-subparallel reflection (Fig. 11). The three bottom current channels are parallel to the coastline in the NE direction, and the strata of gas formation IIIU are divided into three parts (Fig. 12a) from west to east. The western channel is gentle and S-shaped, the curvatures of the central and eastern channels are relatively small, and the three channels are nearly parallel. The width of the channel ranges from 0.5 km to 1.2 km and is slightly narrower in the south, showing a trend of widening and merging to the northeast (Figs 9a, b). The study of the interaction between shallow bottom currents and delta fronts is still in its infancy. The paleocurrent direction of these three Pliocene bottom current channels is speculated to have flowed from south to north, as shown in Fig. 12b.

5.3 *Provenance tracing of detrital zircons*

Wang et al. (2014, 2015, 2019) performed detailed studies on the U-Pb age spectrum identification of detrital zircons in the potential provenance areas of Pliocene–Pleistocene reservoirs in

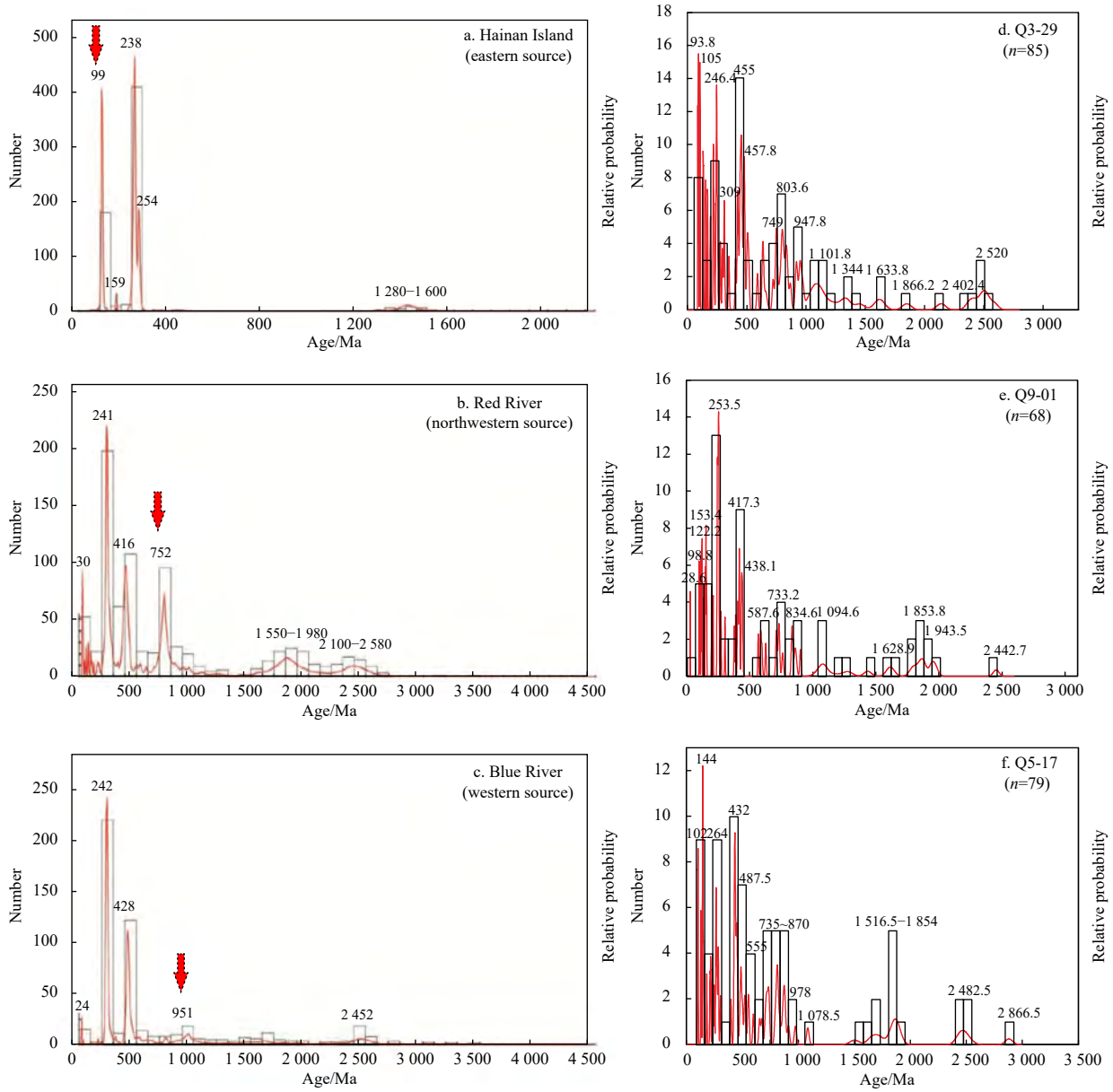

Fig. 13. Comparison of U-Pb ages of detrital zircon from the second member of the Yinggehai Formation in the Dongfang (DF) gas field, Yinggehai Basin, with the age spectra of modern river sediments in the three potential provenance areas of the DF area. a–c are the peak age characteristics of provenances in the eastern, northwestern, and western parts of the study area, respectively (according to Wang et al. (2014, 2015, 2019)); d–f are the U-Pb age distribution characteristics of the Q3-29, Q9-01 and Q5-17 samples in the study area. The red arrows are the marker age peak of each potential source area. The relative probability of a certain age range is represented by the red line.

the YGHB and analyzed the age characteristics of modern sediments of the three potential provenance areas in the YGHB (Figs 13a–c). The main provenance direction of the second member of the YGHF in the DF area also comes from these three provenance areas. According to Fig. 13, Hainan Island provenance has main age peaks of 99 Ma, 238 Ma, 1 280–1 600 Ma, with 99 Ma as the main mark; the Red River provenance in northern Vietnam has many age peaks of 30 Ma, 241 Ma, 752 Ma, 1 550–1 980 Ma, 2 100–2 580 Ma and so on, and 752 Ma is the typical age of Red River provenance; the Blue River provenance in central Vietnam has major age peaks of 242 Ma, 428 Ma, 951 Ma, 2 452 Ma, with 951 Ma as the characteristic age peak. On the whole, the age of detrital zircon from the Red River provenance includes both a young provenance of 30 Ma and an older provenance of 2 580 Ma, a range is wider than that of Hainan Island and the Blue River.

The detrital zircon samples Q3-29, Q5-17 and Q9-01 collected from Wells 3, 5 and 9 in the study area were subjected to LA-ICP-MS U-Pb age testing (Fig. 14). After removing the age samples with harmony <90% and >110%, 85, 68 and 79 effective data points were obtained, respectively (Figs 13d–f). The results

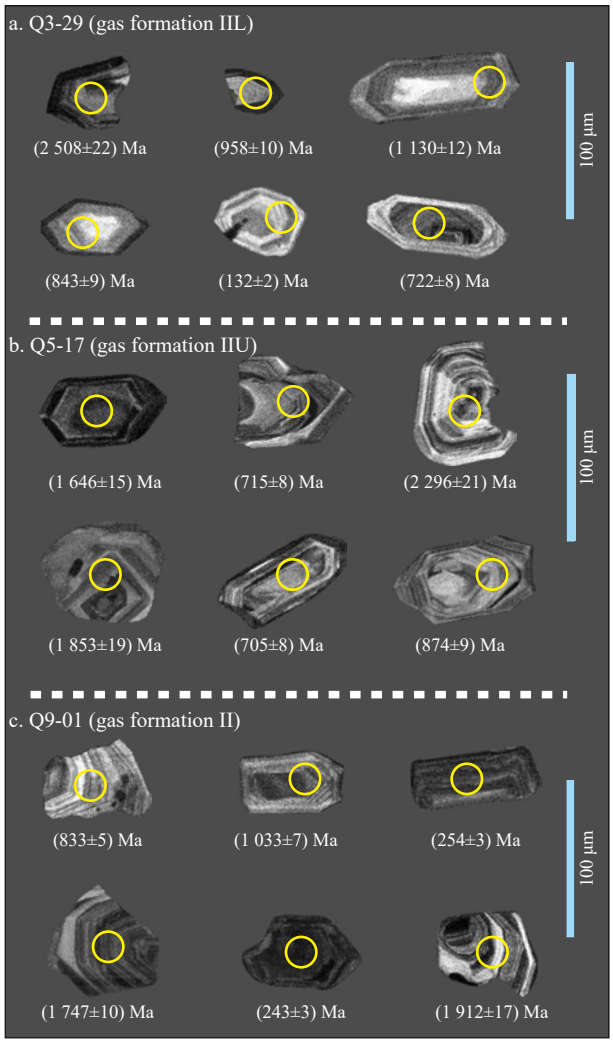

Fig. 14. Zircon cathodoluminescence diagram in the second member of the Yinggehai Formation in the Dongfang gas field, Yinggehai Basin, where $^{206}Pb/^{238}U$ and 1σ corresponding ages are taken for measuring points less than 1 000 Ma, and the corresponding ages of $^{207}Pb/^{206}Pb$ and 1σ are taken for dating points greater than 1 000 Ma.

show that sample Q3-29 has three main peak ages or intervals of 93.8–105 Ma, 246.4 Ma and 455 Ma and four secondary peak ages or intervals of 309 Ma, 749 Ma, 947.8 Ma and 2 402–2 520 Ma. Sample Q9-01 has three main peak ages or intervals of 253.5 Ma, 98.8–153.4 Ma and 417.3 Ma and four secondary peak ages or intervals of 28.6 Ma, 733.2 Ma, 834.6 Ma and 587.6 Ma. Sample Q5-17 has three main peak ages of 144 Ma, 432 Ma and 102 Ma and five secondary peak ages or intervals of 264 Ma, 735–870 Ma, 487.5 Ma, 555 Ma and 1 516.5–1854 Ma.

Compared with the characteristic age peaks of zircon in the three potential source areas, it can be seen that (Fig. 13) (1) sample Q3-29 collected from Well 3 in the easternmost part of the study area is affected by the mixture sources of Red River in northern Vietnam, Blue River in central Vietnam and Hainan Island; (2) sample Q9-01 collected from Well 9 in the southwest of the study area is mainly affected by the provenance of Red River in northern Vietnam and Blue River in central Vietnam; (3) sample Q5-17 collected from Well 5 in the west of the study area is affected by the provenance of Red River in northern Vietnam and the addition of clastic material from Hainan Island in the east, but the provenance is mainly from the north.

In general, zircons in the study area indicate the mixing of clasts from three provenance areas: the Red River, the Blue River and Hainan Island. The provenances of the Red River and the Blue River are consistent with the NW–SE paleocurrent direction indicated by the 3D seismic data, and the clastic material from Hainan Island in the northeastern part of the study area may be transported to the study area by counterclockwise shallow bottom currents and deposited.

5.4 *Establishment of the sedimentary model*

Based on the analysis of the abovementioned lithofacies, logging facies, seismic facies, sedimentary evolution and distribution, this paper concludes that the second member of the YGHF in the DF gas field represents a deltaic-shallow marine sedimentary background and that at least four stages of delta front sand bodies with provenances derived from the Red River in the northwest and the Blue River in the west are developed. The lithologies of the sand bodies are very fine sandstone-coarse siltstone (the particle sizes are between 3 Φ and 5 Φ). The sedimentary period of the four gas formations spanned approximately 1.5 Ma to 2 Ma Vertically, each gas formation is equivalent to a 4th-order sequence with coarsening-upward grains and a shallower water body. Each 4th-order sequence corresponds to a small-scale rapid relative sea level fall, lasting approximately 0.5 Ma. Four 4th-order sequences constitute a 3rd-order sequence. The sequence boundary, i.e., the top surface of gas formation I, is a regional transgressive surface. Large-scale retrogradation reflections and an extensive set of stable mudstones of overlying gas formation 0 indicate a relatively high sea level rise.

Horizontally, numerous bottom currents developed in each sedimentary period, which were distributed in an arc parallel to the coastline, and the underlying sediments were reformed to produce multistage overlapping erosion troughs. The delta front sand bodies and prodelta-continental shelf mudstones deposited in the same period and later periods quickly filled the erosion troughs, and the three large bottom currents that developed from the late stage of gas formation IIU to the early stage of gas formation I are the most typical. Based on the above research results, a comprehensive sedimentary model of the second member of the YGHF can be established, as shown in Fig. 15.

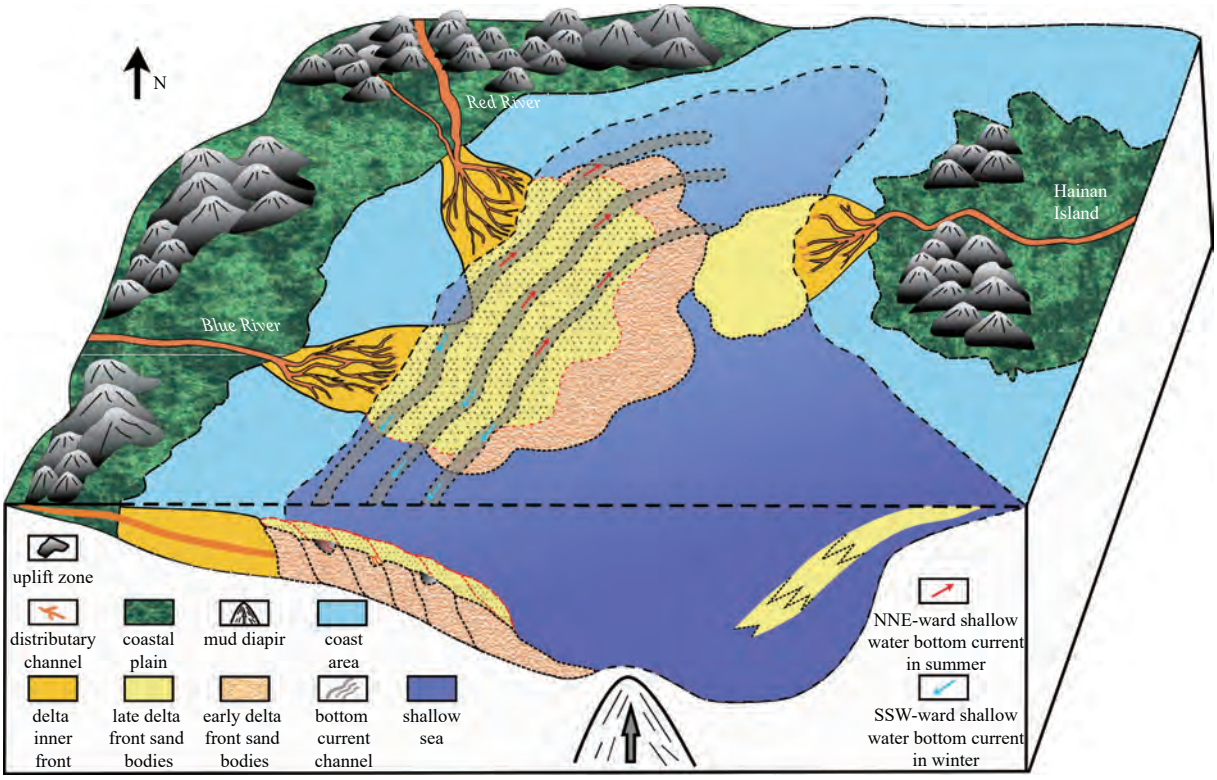

Fig. 15. Comprehensive sedimentary model of the second member of the Yinggehai Formation in the DF1-1 gas field, Yinggehai Basin.

6 Conclusions

(1) The second member of the YGHF in the DF1-1 gas field is a bright spot-type gas reservoir because the sandstone bears gas showing high-amplitude bright spots in the eastern part of the study area. The RMS amplitude does not directly reflect the sedimentary facies information but indicates the gas-bearing range. Sand bodies are well developed in all gas formations, and the distribution of gas reservoirs is obviously controlled by structures, mainly located in the high part of the dome-shaped diapir zone and its periphery. Sandstones with high-amplitude parallel reflections have better gas-bearing properties, and the faults associated with the diapir caused no obvious loss of the gas reservoir.

(2) The second member of the YGHF in the DF1-1-1 gas field is a delta front deposit developed against the background of a shallow marine shelf. The lithologies of the study area are mainly composed of very fine sand and coarse silt, showing a series of reverse cycles of parasequence funnel-type, strong toothed bell-type, and toothed low funnel-type logging facies. There are two typical seismic facies, namely, progradational reflections and erosion channel fills, which correspond to the delta front and bottom current channels, respectively, and they superimpose and interact with each other. When the provenance supply to the delta is strong, the area is dominated by a large set of delta front progradational reflections, while in the period of relative sea level rise, it is dominated by the surface bottom current in the NE direction, and erosion fills are obvious.

(3) Four stages of delta front sand bodies with provenances coming from the Red River in northern Vietnam and the Blue River in central Vietnam have developed in the second member of the YGHF, corresponding to four gas formations from the bottom up, lasting a total of 1.5 Ma to 2 Ma. During the sedimentary period of each gas formation, bottom current channels were developed and distributed along the coastline, and the underlying delta front sediments were reshaped to form superposed deposits of multistage delta fronts and erosion troughs, which were filled with delta front sand bodies or predelta mud, featuring sandy progradation or argillaceous blank fill reflections. The three large-scale bottom current channels that developed in the late stage of gas formation IIU are the most typical. The NE-trending arc-shaped distribution along the coastline strongly reformed the underlying delta front sand bodies.

References

Abreu V, Sullivan M, Pirmez C, et al. 2003. Lateral accretion packages (LAPs): an important reservoir element in deep water sinuous channels. Marine and Petroleum Geology, 20(6–8): 631–648, doi: 10.1016/j.marpetgeo.2003.08.003

Bolli H M, Saunders J B. 1985. Oligocene to Holocene low latitude planknic foraminifera. In: Bolli H M, et al., eds. Planktonic Stratigraphy. Cambridge: Cambridge University Press, 155–262

Brouwer F G C, Welsh A, Connolly D, et al. 2008. High frequencies attenuation and low frequency shadows in seismic data caused by gas chimneys, Onshore Ecuador. In: Proceedings of the 70th EAGE Conference and Exhibition Incorporating SPE EUROPEC 2008. Rome: European Association of Geoscientists & Engineers, cp–40-00060

Cao Licheng, Jiang Tao, Wang Zhenfeng, et al. 2015. Provenance of Upper Miocene sediments in the Yinggehai and Qiongdongnan basins, northwestern South China Sea: evidence from REE, heavy minerals and zircon U–Pb ages. Marine Geology, 361: 136–146, doi: 10.1016/j.margeo.2015.01.007

Carcione J M, Qadrouh A N, Perroud H, et al. 2018. Seismic attenuation, normal moveout stretch, and low-frequency shadows underlying bottom simulating reflector events. Geophysical Prospecting, 66(5): 857–871, doi: 10.1111/1365-2478.12623

Castagna J P, Sun Shengjie, Siegfried R W. 2003. Instantaneous spectral analysis: detection of low-frequency shadows associated with hydrocarbons. The Lead Edge, 22(2): 120–127, doi: 10.1190/1.1559038

Chen C S, Jeng Y. 2011. Nonlinear data processing method for the signal enhancement of GPR data. Journal of Applied Geophysics, 75(1): 113–123, doi: 10.1016/j.jappgeo.2011.06.017

Chen Honghan, Li Sitian, Sun Yongchuan, et al. 1998. Two petroleum systems charge the YA13–1 gas field in Yinggehai and Qiongdongnan basins, South China Sea. AAPG Bulletin, 82(5A): 757–772

Chen Hui, Xie Xinong, van Rooij D, et al. 2014. Depositional characteristics and processes of alongslope currents related to a seamount on the northwestern margin of the Northwest Sub-Basin, South China Sea. Marine Geology, 355: 36–53, doi: 10.1016/j.margeo.2014.05.008

Chen Hui, Xie Xinong, Zhang Wenyan, et al. 2016. Deep-water sedimentary systems and their relationship with bottom currents at the intersection of Xisha Trough and Northwest Sub-Basin, South China Sea. Marine Geology, 378: 101–113, doi: 10.1016/j.margeo.2015.11.002

Faugères J C, Stow D A V. 1993. Bottom-current-controlled sedimentation: a synthesis of the contourite problem. Sedimentary Geology, 82(1–4): 287–297, doi: 10.1016/0037-0738(93)90127-Q

Faugères J C, Stow D A V, Imbert P, et al. 1999. Seismic features diagnostic of contourite drifts. Marine Geology, 162(1): 1–38, doi: 10.1016/S0025-3227(99)00068-7

Fonnesu M, Palermo D, Galbiati M, et al. 2020. A new world-class deep-water play-type, deposited by the syndepositional interaction of turbidity flows and bottom currents: the giant Eocene Coral Field in northern Mozambique. Marine and Petroleum Geology, 111: 179–201, doi: 10.1016/j.marpetgeo.2019.07.047

Gao Zhenzhong, He Youbin, Zhang Xingyang, et al. 2000. Internal-wave and internal-tide deposits of the Middle-Upper Ordovician in the Center Tarim Basin. Acta Sedimentologica Sinica, 18(3): 400–407

Goloshubin G M, Bakulin A V. 1998. Seismic reflectivity of a thin porous fluid-saturated layer versus frequency. In: 1998 SEG Annual Meeting. New Orleans, Louisiana: SEG, 976–979

Gong Chenglin, Wang Yingmin, Rebesco M, et al. 2018. How do turbidity flows interact with contour currents in unidirectionally migrating deep-water channels?. Geology, 46(6): 551–554, doi: 10.1130/G40204.1

Gong Chenglin, Wang Yingmin, Steel R J, et al. 2016a. Flow processes and sedimentation in unidirectionally migrating deep-water channels: from a three-dimensional seismic perspective. Sedimentology, 63(3): 645–661, doi: 10.1111/sed.12233

Gong Chenglin, Wang Yingmin, Zheng Rongcai, et al. 2016b. Middle Miocene reworked turbidites in the Baiyun Sag of the Pearl River Mouth Basin, northern South China Sea margin: Processes, genesis, and implications. Journal of Asian Earth Sciences, 128: 116–129, doi: 10.1016/j.jseaes.2016.06.025

Hao Fang, Dong Weiliang, Zou Huayao, et al. 2004. Effects of overpressured fluid flow on petroleum accumulation in the Yinggehai Basin. Acta Geologica Sinica (English Edition), 78(4): 1011–1018, doi: 10.1111/j.1755-6724.2004.tb00223.x

Hao Fang, Li Sitian, Dong Weiliang, et al. 1998. Abnormal organic-matter maturation in the Yinggehai Basin, South China Sea: implications for hydrocarbon expulsion and fluid migration from overpressured systems. Journal of Petroleum Geology, 21(4): 427–444, doi: 10.1111/j.1747-5457.1998.tb00794.x

Hao Fang, Li Sitian, Gong Zaisheng, et al. 2000. Thermal regime, interreservoir compositional heterogeneities, and reservoir-filling history of the Dongfang Gas Field, Yinggehai Basin, South China Sea: evidence for episodic fluid injections in overpressured basins?. AAPG Bulletin, 84(5): 607–626, doi: 10.1306/C9EBCE69-1735-11D7-8645000102C1865D

Hao Fang, Li Sitian, Gong Zaisheng, et al. 2002. Mechanism of diapirism and episodic fluid injections in the Yinggehai Basin. Science in China Series D: Earth Sciences, 45(2): 151–159, doi: 10.1007/BF02879792

Hao Fang, Li Sitian, Sun Yongchuan, et al. 1996. Characteristics and origin of the gas and condensate in the Yinggehai Basin, offshore South China Sea: evidence for effects of overpressure on petroleum generation and migration. Organic Geochemistry, 24(3): 363–375, doi: 10.1016/0146-6380(96)00009-5

Hao Fang, Sun Yongchuan, Li Sitian, et al. 1995. Overpressure retardation of organic-matter maturation and petroleum generation: a case study from the Yinggehai and Qiongdongnan Basins, South China Sea. AAPG Bulletin, 79(4): 551–562, doi: 10.1306/8D2B158E-171E-11D7-8645000102C1865D

He Youbin, Gao Zhenzhong, Luo Shunshe, et al. 2007. Discovery of Internal-tide deposits from the Third Member of Pingliang Formation in Longxian Area, Shaanxi province. Journal of Oil and Gas Technology, 29(4): 28–33

He Weijun, Xie Jinyou, Liu Xinyu, et al. 2011. Foraminiferal biostratigraphy and sedimentary environment reconstruction based on paleontological data from bore hole DF1–1–11, Yinggehai Basin. Journal of Stratigraphy, 35(1): 84–90

He Zhenhua, Xiong Xiaojun, Bian Lien. 2008. Numerical simulation of seismic low-frequency shadows and its application. Applied Geophysics, 5(4): 301–306, doi: 10.1007/s11770-008-0040-4

Hedlin K, Mewhort L, Margrave G. 2001. Delineation of steam flood using seismic attenuation. In: SEG Technical Program Expanded Abstracts 2001. Tulsa, Oklahoma: Society of Exploration Geophysicist, 1572–1575

Huang Yintao, Wen Li, Yao Guangqing, et al. 2018. Sedimentary characteristics of thick fine-grained shallow-marine gravity flow deposits from Huangliu Formation in Dongfang area, Yinggehai Basin, China. Acta Petrolei Sinica, 39(3): 290–303

Huang Baojia, Xiao Xianming, Dong Weiliang. 2002. Multiphase natural gas migration and accumulation and its relationship to diapir structures in the DF1-1 Gas Field, South China Sea. Marine and Petroleum Geology, 19(7): 861–872, doi: 10.1016/S0264-8172(02)00109-5

Huang Baojia, Xiao Xianming, Hu Zhongliang, et al. 2005. Geochemistry and episodic accumulation of natural gases from the Ledong gas field in the Yinggehai Basin, offshore South China Sea. Organic Geochemistry, 36(12): 1689–1702, doi: 10.1016/j.orggeochem.2005.08.011

Huang Baojia, Xiao Xianming, Li Xuxuan. 2003. Geochemistry and origins of natural gases in the Yinggehai and Qiongdongnan basins, offshore South China Sea. Organic Geochemistry, 34(7): 1009–1025, doi: 10.1016/S0146-6380(03)00036-6

Huang Baojia, Xiao Xianming, Li Xushen, et al. 2009. Spatial distribution and geochemistry of the nearshore gas seepages and their implications to natural gas migration in the Yinggehai Basin, offshore South China Sea. Marine and Petroleum Geology, 26(6): 928–935, doi: 10.1016/j.marpetgeo.2008.04.009

Jiang Tao, Cao Licheng, Xie Xinong, et al. 2015. Insights from heavy minerals and zircon U–Pb ages into the middle Miocene–Pliocene provenance evolution of the Yinggehai Basin, northwestern South China Sea. Sedimentary Geology, 327: 32–42, doi: 10.1016/j.sedgeo.2015.07.011

Jiang Ping, Yu Xinghe, Huang Yueyin, et al. 2012. Application of reservoir characterization techniques in DF1–1 Gas field. Earth Science Frontiers, 19(2): 87–94

Lei Chao, Ren Jianye, Sternai P, et al. 2015. Structure and sediment budget of Yinggehai–Song Hong Basin, South China Sea: implications for Cenozoic tectonics and river basin reorganization in Southeast Asia. Tectonophysics, 22: 177–190, doi: 10.1016/j.tecto.2015.05.024

Li Xuejie, Chen Fang, Chen Chaoyun, et al. 2004. Quantitative research on relationship between planktonic foraminifera content and water depth in western South China Sea. Journal of Palaeogeography, 6(4): 442–447

Li Sitian, Lin Changsong, Zhang Qiming, et al. 1999. Episodic rifting of continental marginal basins and tectonic events since 10 Ma in the South China Sea. Chinese Science Bulletin, 44(1): 10–23, doi: 10.1007/BF03182877

Li Hua, Wang Yingmin, Zhu Weilin, et al. 2013. Seismic characteristics and processes of the Plio-Quaternary unidirectionally migrating channels and contourites in the northern slope of the South China Sea. Marine and Petroleum Geology, 43: 370–380, doi: 10.1016/j.marpetgeo.2012.12.010

Li Shengli, Yu Xinghe, Xie Yuhong, et al. 2010. Mud flow gully identi-

fication mark, type and depositional model in the littoral and neritic marine: a case study of Dongfang 1-1 gas field in Yinggehai Basin. Acta Sedimentologica Sinica, 28(6): 1076–1080

Li Yufeng, Zhang Gongcheng, Pu Renhai, et al. 2021. Characteristics and origins of middle Miocene mounds and channels in the northern South China Sea. Acta Oceanologica Sinica, 40(2): 65–80, doi: 10.1007/s13131-021-1759-5

Liu Meng, Wang Yonghong, Li Sanzhong. 2015a. The distribution pattern and evolution mechanism of winter paleocurrents in South China Sea since Late Pleistocene. Marine Geology & Quaternary Geology, 35(5): 87–94

Liu Xiaofeng, Zhang Daojun, Zhai Shikui, et al. 2015b. A heavy mineral viewpoint on sediment provenance and environment in the Qiongdongnan Basin. Acta Oceanologica Sinica, 34(4): 41–55, doi: 10.1007/s13131-015-0648-1

Lu Hongying, Cheng Bingjie, Shen Zhongmin, et al. 2013. Gas and water reservoir differentiation by time-frequency analysis: a case study in Southwest China. Acta Geodaetica et Geophysica, 48(4): 439–450, doi: 10.1007/s40328-013-0031-7

Luan Xiwu, Lu Yintao, Fan Guozhang, et al. 2021. Deep-water sedimentation controlled by interaction between bottom current and gravity flow: a case study of Rovuma Basin, East Africa. Journal of African Earth Sciences, 180: 104228, doi: 10.1016/j.jafrearsci.2021.104228

Luo Xiaorong, Dong Weiliang, Yang Jihai, et al. 2003. Overpressuring mechanisms in the Yinggehai Basin, South China Sea. AAPG Bulletin, 87(4): 629–645, doi: 10.1306/10170201045

Lü Ming. 2002. A new discussion on lowstand deposition models in Ying-Qiong Basin. China Offshore Oil and Gas (Geology), 16(4): 4–13

Lüdmann T, Wong H K, Berglar K. 2005. Upward flow of North Pacific Deep Water in the northern South China Sea as deduced from the occurrence of drift sediments. Geophysical Research Letters, 32(5): L05614, doi: 10.1029/2004GL021967

Massé L, Faugères J C, Hrovatin V. 1998. The interplay between turbidity and contour current processes on the Columbia Channel fan drift, Southern Brazil Basin. Sedimentary Geology, 115(1–4): 111–132, doi: 10.1016/S0037-0738(97)00089-4

Mulder T, Faugères J C, Gonthier E. 2008. Mixed turbidite—contourite Systems. Developments in Sedimentology, 60: 435–456, doi: 10.1016/S0070-4571(08)10021-8

Mulder T, Lecroart P, Hanquiez V, et al. 2006. The western part of the Gulf of Cadiz: Contour currents and turbidity currents interactions. Geo-Marine Letters, 26(1): 31–41, doi: 10.1007/s00367-005-0013-z

Mullins H T, Keller G H, Kofond J W, et al. 1982. Geology of Great Abaco Submarine Canyon (Blake Plateau): Observations from the research submersible "Alvin". Marine Geology, 48(3–4): 239–257, doi: 10.1016/0025-3227(82)90099-8

Qu Tangdong, Lindstrom E J. 2004. Northward intrusion of Antarctic intermediate water in the western Pacific. Journal of Physical Oceanography, 34(9): 2104–2118, doi: 10.1175/1520-0485(2004)034<2104:NIOAIW>2.0.CO;2

Ren Jianye, Lei Chao, Wang Shan, et al. 2013. Tectonic stratigraphic framework of the Yinggehai—Qiongdongnan Basins and its Implication for tectonics province division in South China Sea. Chinese Journal of Geophysics, 54(6): 1124–1137, doi: 10.1002/cjg2.1689

Schopf T J M. 1981. *Currents in submarine canyons and other sea-valleys*. By F. P. Shepard, N. F. Marshall, P. A. McLoughlin, G. G. Sullivan. Tulsa, OK: American Association of Petroleum Geologists, 1979. 173 pages, 125 figs.. The Journal of Geology, 89(1): 140–141, doi: 10.1086/628573

Shanmugam G. 2000. 50 years of the turbidite paradigm (1950s—1990s): deep-water processes and facies models—a critical perspective. Marine and Petroleum Geology, 17(2): 285–342, doi: 10.1016/S0264-8172(99)00011-2

Shanmugam G. 2003. Deep-marine tidal bottom currents and their reworked sands in modern and ancient submarine canyons. Marine and Petroleum Geology, 20(5): 471–491, doi: 10.1016/S0264-8172(03)00063-1

Shao Lei, Li Xuejie, Geng Jianhua, et al. 2007. Deep water bottom current deposition in the northern South China Sea. Science in China Series D: Earth Sciences, 50(7): 1060–1066, doi: 10.1007/s11430-007-0015-y

Sheriff R E, Geldart L P. 1995. Exploration Seismology. 2nd ed. Cambridge: Cambridge University Press, 416

Stow D A V, Faugères J C, Howe J A, et al. 2002. Bottom currents, contourites and deep-sea sediment drifts: current state-of-the-art. In: Stow D A V, Pudsey C J, Howe J A, et al., eds. Deep-Water Contourite Systems: Modern Drifts and Ancient Series, Seismic and Sedimentary Characteristics. London: Geological Society, 7–20, doi: 10.1144/GSL.MEM.2002.022.01.02

Sun Qiliang, Cartwright J, Lüdmann T, et al. 2017. Three-dimensional seismic characterization of a complex sediment drift in the South China Sea: evidence for unsteady flow regime. Sedimentology, 64(3): 832–853, doi: 10.1111/sed.12330

Sun Qiliang, Cartwright J, Wu Shiguo, et al. 2016. Submarine erosional troughs in the northern South China Sea: Evidence for Early Miocene deepwater circulation and paleoceanographic change. Marine and Petroleum Geology, 77: 75–91, doi: 10.1016/j.marpetgeo.2016.06.005

Sun Ming, Wang Hua, Liao Jihua, et al. 2014. Sedimentary characteristics and model of gravity flow depositional system for the first member of upper Miocene Huangliu Formation in Dongfang area, Yinggehai Basin, northwestern South China Sea. Journal of Earth Science, 25(3): 506–518, doi: 10.1007/s12583-014-0451-5

Sun Zhen, Wang Zhenfeng, Sun Zhipeng, et al. 2015. Structure and kinematic analysis of the deepwater area of the Qiongdongnan Basin through a seismic interpretation and analogue modeling experiments. Acta Oceanologica Sinica, 34(4): 32–40, doi: 10.1007/s13131-015-0585-z

Tian Jie, Wu Shiguo, Lv Fuliang, et al. 2015. Middle Miocene mound-shaped sediment packages on the slope of the Xisha carbonate platforms, South China Sea: combined result of gravity flow and bottom current. Deep-Sea Research Part II: Topical Studies in Oceanography, 122: 172–184, doi: 10.1016/j.dsr2.2015.06.016

Viana A R, Faugères J C, Stow D A V. 1998. Bottom-current-controlled sand deposits — a review of modern shallow- to deep-water environments. Sedimentary Geology, 115(1–4): 53–80, doi: 10.1016/S0037-0738(97)00087-0

Wade B S. 2004. Planktonic foraminiferal biostratigraphy and mechanisms in the extinction of Morozovella in the late middle Eocene. Marine Micropaleontology, 51(1–2): 23–38, doi: 10.1016/j.marmicro.2003.09.001

Wang Xinguo, He Jiankun, Ding Lin, et al. 2013. A possible mechanism for the initiation of the Yinggehai Basin: a visco-elasto-plastic model. Journal of Asian Earth Sciences, 74: 25–36, doi: 10.1016/j.jseaes.2013.05.022

Wang Zhenfeng, Huang Baojia. 2008. Dongfang 1–1 gas field in the mud diapir belt of the Yinggehai Basin, South China Sea. Marine and Petroleum Geology, 25(4–5): 445–455, doi: 10.1016/j.marpetgeo.2008.01.004

Wang Pinxian, Li Qianyu. 2009. Oceanographical and geological background. In: Wang Pinxian, Li Qianyu, eds. The South China Sea: Paleoceanography and Sedimentology. Dordrecht: Springer Netherlands, 25–73

Wang Ce, Liang Xinquan, Foster D A, et al. 2019. Detrital zircon ages: a key to unraveling provenance variations in the eastern Yinggehai–Song Hong Basin, South China Sea. AAPG Bulletin, 103(7): 1525–1552, doi: 10.1306/11211817270

Wang Ce, Liang Xinquan, Fu Jiangang, et al. 2015. Detrital zircon provenance of Pliocene Yinggehai Formation in the Ledong Gas Field of the Yinggehai-Song Hong basin. Acta Geologica Sinica (English Edition), 87(S1): 279–280

Wang Ce, Liang Xinquan, Xie Yuhong, et al. 2014. Provenance of Upper Miocene to Quaternary sediments in the Yinggehai-Song Hong Basin, South China Sea: evidence from detrital zircon U–Pb ages. Marine Geology, 355: 202–217, doi: 10.1016/j.margeo.2014.06.004

Wang Xingxing, Zhuo Haiteng, Wang Yingmin, et al. 2018. Controls of

contour currents on intra-canyon mixed sedimentary processes: insights from the Pearl River Canyon, northern South China Sea. Marine Geology, 406: 193–213, doi: 10.1016/j.margeo.2018.09.016

Wei Zhou, Wang Yingmin, Gao Xianzhi, et al. 2015. Architecture, evolution history and controlling factors of the Baiyun submarine canyon system from the middle Miocene to Quaternary in the Pearl River Mouth Basin, northern South China Sea. Marine and Petroleum Geology, 67: 389–407, doi: 10.1016/j.marpetgeo.2015.05.015

Xie Yuhong, Huang Baojia. 2014. Characteristics and accumulation mechanisms of the Dongfang 13–1 high temperature and overpressured gas field in the Yinggehai Basin, the South China Sea. Science China Earth Sciences, 57(11): 2799–2807, doi: 10.1007/s11430-014-4934-0

Xie Xinong, Li Sitian, Dong Weiliang, et al. 2001. Evidence for episodic expulsion of hot fluids along faults near diapiric structures of the Yinggehai Basin, South China Sea. Marine and Petroleum Geology, 18(6): 715–728, doi: 10.1016/S0264-8172(01)00024-1

Xie Xinong, Müller R D, Li Sitian, et al. 2006. Origin of anomalous subsidence along the northern South China Sea margin and its relationship to dynamic topography. Marine and Petroleum Geology, 23(7): 745–765, doi: 10.1016/j.marpetgeo.2006.03.004

Xu Weihai, Yan Wen, Chen Zhong, et al. 2014. Organic matters and lipid biomarkers in surface sediments from the northern South China Sea: Origins and transport. Journal of Earth Science, 25(1): 189–196, doi: 10.1007/s12583-014-0412-z

Yan Yi, Carter A, Palk C, et al. 2011. Understanding sedimentation in the Song Hong–Yinggehai Basin, South China Sea. Geochemistry, Geophysics, Geosystems, 12(6): Q06014, doi: 10.1029/2011GC003533

Yang Fengli, Zhou Zuyi, Zhang Na, et al. 2013. Stress field modeling of northwestern South China Sea since 5.3 Ma and its tectonic significance. Acta Oceanologica Sinica, 32(12): 31–39, doi: 10.1007/s13131-013-0385-2

Yue Shaofei, Zhang Hui, Wang Qingshuai, et al. 2017. Turbidite Sand: a new view on sedimentary facies of Pliocene Zhujiang Member-2 in DF-A Gas Field, Yinggehai Basin. Marine Origin Petroleum Geology, 22(4): 11–18

Yue Shaofei, Zhang Hui, Yang Zhaoqiang, et al. 2018. Analysis of formation mechanism of the lateral accretion packages in the Yinggehai Formation under the background of shallow sea in Dongfang A Gasfield, Yinggehai Basin. Petroleum Geology and Recovery Efficiency, 25(6): 32–37

Zeng Hongliu. 2010. Geologic significance of anomalous instantaneous frequency. Geophysics, 75(3): P23–P30, doi: 10.1190/1.3427638

Zhang Qiming, Hao Fang. 1997. Evolution and petroleum systems of the Ying-Qiong Basin. Science in China Series D: Earth Sciences, 40(5): 553–560, doi: 10.1007/BF02877623

Zhang Huolan, Pei Jianxiang, Zhang Yingzhao, et al. 2013. Overpressure reservoirs of the Huangliu Formation of the Dongfang area, Yinggehai Basin, South China Sea. Petroleum Exploration and Development, 40(3): 305–315, doi: 10.1016/S1876-3804(13)60037-3

Zhao Quanhong, Li Qianyu, Jian Zhimin. 2009. Deep waters and oceanic connection. In: Wang Pinxian, Li Qianyu, eds. The South China Sea: Paleoceanography and Sedimentology. Dordrecht: Springer, 395–437

Zheng Xufeng, Kao S, Chen Zhong, et al. 2016. Deepwater circulation variation in the South China Sea since the Last Glacial Maximum. Geophysical Research Letters, 43(16): 8590–8599, doi: 10.1002/2016GL070342

Zheng Hongbo, Yan Pin. 2012. Deep-water bottom current research in the northern South China Sea. Marine Georesources & Geotechnology, 30(2): 122–129, doi: 10.1080/1064119X.2011.586015

Zhu Mangzheng, Graham S, Pang Xiong, et al. 2010. Characteristics of migrating submarine canyons from the middle Miocene to present: implications for paleoceanographic circulation, northern South China Sea. Marine and Petroleum Geology, 27(1): 307–319, doi: 10.1016/j.marpetgeo.2009.05.005

Zhuo Haiteng, Wang Yingmin, Xu Qiang, et al. 2013. Sedimentary characteristics and genesis of lateral accretion packages in the Pliocene of Dongfang area of Yinggehai Basin in northern South China Sea. Journal of Palaeogeography, 15(6): 787–794